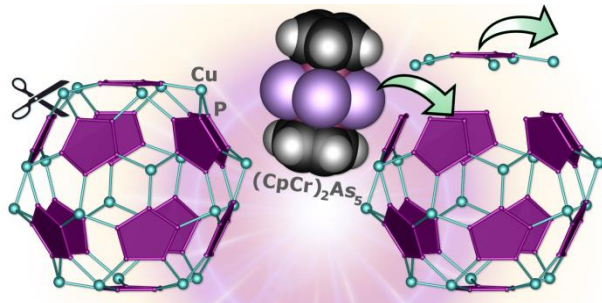


Supplementary information for the manuscript

From Nano-Balls to Nano-Bowls

Helena Brake, Claudia Heindl, Eugenia Peresypkina, Alexander V. Virovets, Werner Kremer,
Manfred Scheer*



1. Contents

1 Experimental Part	2
General Remarks:	2
Synthesis of $[(\text{CpCr})_2(\mu,\eta^{5:5}\text{-As}_5)] @ [(\text{Cp}^*\text{Fe}(\eta^5\text{-P}_5))_{11}(\text{CuCl})_{13.5}] \cdot 8 \text{CH}_2\text{Cl}_2 \cdot 0.5 \text{CH}_3\text{CN}$ (1@2a) · 8 CH ₂ Cl ₂ · 0.5 CH ₃ CN)	2
.....	2
Synthesis of $[(\text{CpCr})_2(\mu,\eta^{5:5}\text{-As}_5)] @ [(\text{Cp}^*\text{Fe}(\eta^5\text{-P}_5))_{11}(\text{CuBr})_{12.5}] \cdot 2 \text{CH}_2\text{Cl}_2$ (1@2b) · 2 CH ₂ Cl ₂)	3
Synthesis of $[\text{CpCr}(\mu,\eta^5\text{-As}_5)] @ [(\text{Cp}^*\text{Fe}(\eta^5\text{-P}_5))_{12}(\text{CuCl})_{20}]$ ($[\text{CpCr}(\mu,\eta^5\text{-As}_5)] @ \text{B}$)	4
2 Spectra	5
3 Crystallographic Details.....	13
Table S1 Experimental details for compounds 1, 1@2a and 1@2b	14
Crystal structure of 1	15
Table S2. Selected geometric parameters of 1	16
Crystal structure of compounds 2a and 2b.....	16
Table S3. Selected geometric parameters of 2a	17
Table S4. Selected geometric parameters of 2b	20
4 Solid solutions of supramolecules	23
Table S5. Individual supramolecules in 1@2a and 1@2b: a reconstruction	24
Table S6. Individual supramolecules 1@2a or 1@2b and some of their solid solutions	25
5 Inorganic scaffolds: a comparison.....	27

1 Experimental Part

General Remarks:

All reactions were performed under an inert atmosphere of dry nitrogen or argon with standard vacuum, Schlenk and glove-box techniques. Solvents were purified, dried and degassed prior to use by standard procedures. $[(\text{CpCr})_2(\mu,\eta^{5:5}\text{-As}_5)]$ ^[1] and $[\text{Cp}^*\text{Fe}(\eta^5\text{-P}_5)]$ ^[2] were synthesized following reported procedures. CuCl and CuBr are commercially available and were used without further purification. Solution NMR spectra were recorded on a BRUKER Avance 400 (^1H : 400.130 MHz; $^{31}\text{P}\{^1\text{H}\}$: 161.976 MHz). Chemical shifts δ are given in [ppm] referring to external standards of tetramethylsilane (^1H NMR spectra) or 85% phosphoric acid ($^{31}\text{P}\{^1\text{H}\}$ NMR spectra). MAS NMR spectra were acquired on a Bruker Avance 300 spectrometer. ESI-MS and EI-MS spectra were recorded on a ThermoQuest Finnigan MAT TSQ 7000 and on a Finnigan MAT 95 mass spectrometer, respectively. Elemental analyses were determined by Mikroanalytisches Labor, Lehrbereich Anorganische Chemie, TU Munich for all elements. EPR spectroscopy was carried out on a MiniScope MS400 device with a frequency of 9.44 GHz.

Synthesis of $[(\text{CpCr})_2(\mu,\eta^{5:5}\text{-As}_5)]@[\{\text{Cp}^*\text{Fe}(\eta^5\text{-P}_5)\}_{11}(\text{CuCl})_{13.5}] \cdot 8 \text{CH}_2\text{Cl}_2 \cdot 0.5 \text{CH}_3\text{CN}$ (1@2a · 8 CH₂Cl₂ · 0.5 CH₃CN)

$[\text{Cp}^*\text{Fe}(\eta^5\text{-P}_5)]$ (102 mg, 0.30 mmol) and 1 (19 mg, 0.031 mmol) are dissolved in CH₂Cl₂ (22 mL). After treatment in a warm ultrasonic bath (1 h, 60°C, 35 kHz), the dark green solution is filtered into a thick Schlenk tube and carefully layered with a colorless solution of CuCl (64 mg, 0.65 mmol) in CH₃CN (22 mL). After 1-2 weeks, the mother liquor is decanted and the crystals are washed three times each with CH₂Cl₂/CH₃CN (2:1) and pentane and dried.

Analytical data of 1@2a:

Yield: 72 mg (11 µmol, 42%)

Elemental analysis: Calculated (%) for

$[(\text{CpCr})_2(\mu,\eta^{5:5}\text{-As}_5)]@[\{\text{Cp}^*\text{Fe}(\eta^5\text{-P}_5)\}_{11}(\text{CuCl})_{13.5}] \cdot 8 \text{CH}_2\text{Cl}_2 \cdot 0.5 \text{CH}_3\text{CN}$ (6451 g/mol): C 24.02, H 3.01, N 0.11, Cu 13.30, P 26.41; found (%): C 23.88, H 3.35, N 0.07, Cu 13.4, P 26.81.

^1H MAS NMR: δ [ppm] = -13.6 (br), 1.4 (s, br), 6.7 (s, br), 16.4 (br), 21.3 (s, br).

$^{31}\text{P}\{^1\text{H}\}$ MAS NMR: δ [ppm] = 74 (br), 125 (br); a small shoulder at 150 ppm is detected, which can most probably be assigned to free $[\text{Cp}^*\text{Fe}(\eta^5\text{-P}_5)]$.

^1H NMR (CD₂Cl₂): δ [ppm] = 1.42 (s, br), 1.43 (s, br), 1.97 (s, CH₃CN), 2.08 (s, br), 2.18 (s, br), 2.20 (s, br), 3.26 (s, br), 3.33 (s, br).

$^{31}\text{P}\{^1\text{H}\}$ NMR (CD₂Cl₂): δ [ppm] = 60 (br), 120 (br), 152.2 (s, $[\text{Cp}^*\text{Fe}(\eta^5\text{-P}_5)]$); signals almost below noise floor.

¹H NMR (pyridine-d₅): δ [ppm] = 1.33 (s, [Cp*Fe(η⁵-P₅)]), 1.87 (s, CH₃CN), 23.9 (s, br, [(CpCr)₂(μ,η^{5:5}-As₅)]).

³¹P{¹H} NMR (pyridine-d₅): δ [ppm] = 150.5 (s, [Cp*Fe(η⁵-P₅)]).

EI-MS (70 eV): 608.5668 [(CpCr)₂(μ,η^{5:5}-As₅)], 345.9187 [Cp*Fe(η⁵-P₅)], 299.6829 [As₄], 283.9715 [{Cp*Fe(η⁵-P₅)}-P₂].

Positive ion ESI-MS (CH₂Cl₂/CH₃CN): m/z = 2635.4 [{Cp*Fe(η⁵-P₅)}₄Cu₁₃Cl₁₂]⁺, 2535.5 [{Cp*Fe(η⁵-P₅)}₄Cu₁₂Cl₁₁]⁺, 2337.7 [{Cp*Fe(η⁵-P₅)}₄Cu₁₀Cl₉]⁺, 1794.0 [{Cp*Fe(η⁵-P₅)}₃Cu₈Cl₇]⁺, 1744.0 [{Cp*Fe(η⁵-P₅)}₄Cu₄Cl₃]⁺, 1694.1 [(Cp*Fe(η⁵-P₅))₃Cu₇Cl₆]⁺, 1596.2 [{Cp*Fe(η⁵-P₅)}₃Cu₆Cl₅]⁺, 952.6 [{Cp*Fe(η⁵-P₅)}₂Cu₃Cl₂]⁺, 854.7 [{Cp*Fe(η⁵-P₅)}₂Cu₂Cl]⁺, 754.8 [(Cp*Fe(η⁵-P₅))₂Cu]⁺, 490.9 [{Cp*Fe(η⁵-P₅)}Cu(CH₃CN)₂]⁺, 449.9 [{Cp*Fe(η⁵-P₅)}Cu(CH₃CN)]⁺, 408.9 [{Cp*Fe(η⁵-P₅)}Cu]⁺.

Negative ion ESI-MS (CH₂Cl₂/CH₃CN): m/z = 232.8 [Cu₂Cl₃]⁻.

Synthesis of [(CpCr)₂(μ,η^{5:5}-As₅)]@[{Cp*Fe(η⁵-P₅)}₁₁(CuBr)_{12.5}] · 2 CH₂Cl₂ (1@2b · 2 CH₂Cl₂)

[Cp*Fe(η⁵-P₅)] (106 mg, 0.31 mmol) and 1 (21 mg, 0.034 mmol) are dissolved in CH₂Cl₂ (21 mL). After treatment in a warm ultrasonic bath (1 h, 60°C, 35 kHz), the dark green solution is filtered into a thick Schlenk tube and carefully layered with a colorless solution of CuBr (87 mg, 0.61 mmol) in CH₃CN (21 mL). After 1-2 weeks, the mother liquor is decanted and the crystals are washed three times each with CH₂Cl₂/CH₃CN (2:1) and pentane and dried.

Analytical data of 1@2b:

Yield: 122 mg (19 μmol, 67%)

Elemental analysis: Calculated (%) for

[(CpCr)₂(μ,η^{5:5}-As₅)]@[{Cp*Fe(η⁵-P₅)}₁₁(CuBr)_{12.5}] · 2 CH₂Cl₂ (6377 g/mol): C 22.98, H 2.83, Cu 12.46, P 26.71; found (%): C 23.01, H 2.90, Cu 12.44, P 26.77.

¹H MAS NMR: δ [ppm] = -13.4 (br), 1.4 (s, br), 6.8 (s, br), 16.2 (br), 21.3 (s, br).

³¹P{¹H} MAS NMR: δ [ppm] = 70 (br), 126 (br).

¹H NMR (CDCl₃): δ [ppm] = 1.44 (s, br), 1.48 (s, br), 1.49 (s, br), 2.13 (s, br), 2.14 (s, CH₃CN), 2.25 (s, br), 3.32 (s, br), 3.40 (s, br).

³¹P{¹H} NMR (CDCl₃): δ [ppm] = 152.8 (s, [Cp*Fe(η⁵-P₅)]).

¹H NMR (pyridine-d₅): δ [ppm] = 1.33 (s, [Cp*Fe(η⁵-P₅)]), 1.87 (s, CH₃CN), 5.69 (s, CH₂Cl₂), 24.0 (s, br, [(CpCr)₂(μ,η^{5:5}-As₅)]).

³¹P{¹H} NMR (pyridine-d₅): δ [ppm] = 150.5 (s, [Cp*Fe(η⁵-P₅)]).

EI-MS (70 eV): 608.5667 [(CpCr)₂(μ,η^{5:5}-As₅)], 345.9197 [Cp*Fe(η⁵-P₅)], 299.6853 [As₄], 283.9724 [{Cp*Fe(η⁵-P₅)}-P₂].

Positive ion ESI-MS (CH₂Cl₂/CHCl₃/CH₃CN): m/z = 1042.4600 [{Cp*Fe(η⁵-P₅)}₂Cu₃Br₂]⁺, 898.6152 [{Cp*Fe(η⁵-P₅)}₂Cu₂Br]⁺, 754.7710 [{Cp*Fe(η⁵-P₅)}₂Cu]⁺, 449.8758 [{Cp*Fe(η⁵-P₅)}Cu(CH₃CN)]⁺.

Negative ion ESI-MS ($\text{CH}_2\text{Cl}_2/\text{CHCl}_3/\text{CH}_3\text{CN}$): $m/z = 222.7643$ $[\text{CuBr}_2]^-$, 178.8144 $[\text{CuClBr}]^-$, 134.8649 $[\text{CuCl}_2]^-$.

Synthesis of $[\text{CpCr}(\mu,\eta^5\text{-As}_5)]@\{[\text{Cp}^*\text{Fe}(\eta^5\text{-P}_5)\}_{12}(\text{CuCl})_{20}\}$ ($[\text{CpCr}(\mu,\eta^5\text{-As}_5)]@\text{B}$)

$[\text{Cp}^*\text{Fe}(\eta^5\text{-P}_5)]$ (105 mg, 0.30 mmol) and **1** (23 mg, 0.038 mmol) are dissolved in toluene (26 mL). After treatment in a warm ultrasonic bath (1 h, 50°C, 35 kHz), the dark green solution is filtered into a thick Schlenk tube and carefully layered with a colorless solution of CuCl (58 mg, 0.59 mmol) in CH_3CN (20 mL). After 2-3 weeks, the mother liquor is decanted and the crystals are washed twice with toluene/ CH_3CN (1:1) and dried.

Analytical data of $[\text{CpCr}(\mu,\eta^5\text{-As}_5)]@\text{B}$:

Yield: 44 mg (6.6 μmol , 26%)

$^1\text{H NMR}$ (CD_2Cl_2): δ [ppm] = 1.42 (s, br), 1.43 (s, br), 2.08 (s, br), 2.17 (s, br), 2.34 (s, C_7H_8), 3.26 (s, br), 3.33 (s, br), 7.14-7.26 (m, C_7H_8), 19.8 (s, br), 21.3 (s, br).

$^{31}\text{P}\{^1\text{H}\}$ NMR (CD_2Cl_2): δ [ppm] = 69 (br), 120 (br), 151.5 (s, $[\text{Cp}^*\text{Fe}(\eta^5\text{-P}_5)]$); signals almost below noise floor.

$^1\text{H NMR}$ (pyridine-d₅): δ [ppm] = 1.35 (s, $[\text{Cp}^*\text{Fe}(\eta^5\text{-P}_5)]$), 1.84 (s, CH_3CN), 2.23 (s, C_7H_8), 6.0 (br), 23.9 (s, br, $[(\text{CpCr})_2(\mu,\eta^{5:5}\text{-As}_5)]$).

$^{31}\text{P}\{^1\text{H}\}$ NMR (pyridine-d₅): δ [ppm] = 147.2 (s, $[\text{Cp}^*\text{Fe}(\eta^5\text{-P}_5)]$).

EPR-spectrum (crystals, quartz tube, r.t.):

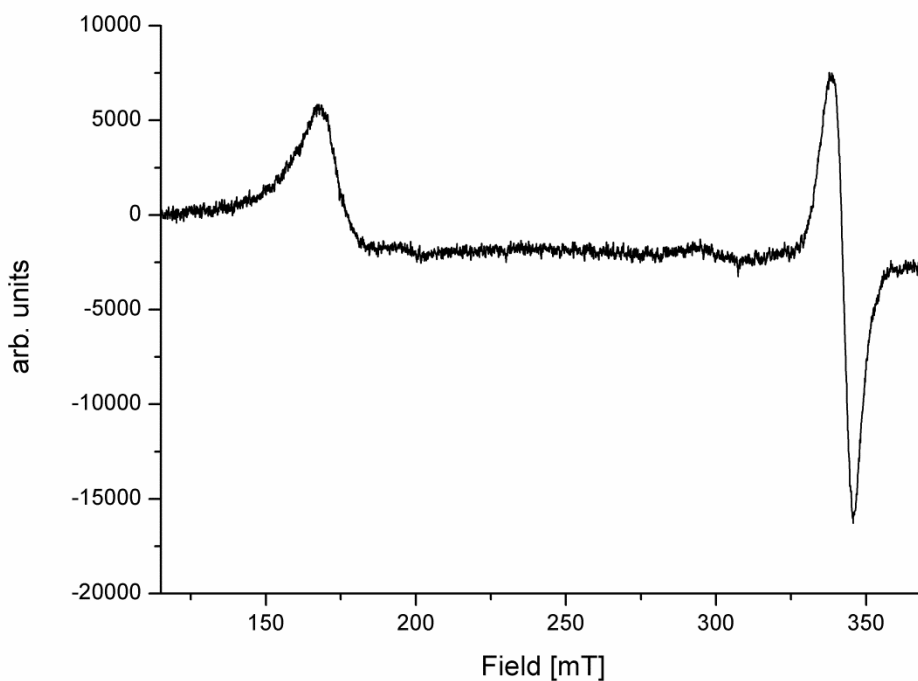


Fig. S1. EPR spectrum of crystals of $[\text{CpCr}(\mu,\eta^5\text{-As}_5)]@\text{B}$ at r.t. (quartz tube).

2 Spectra

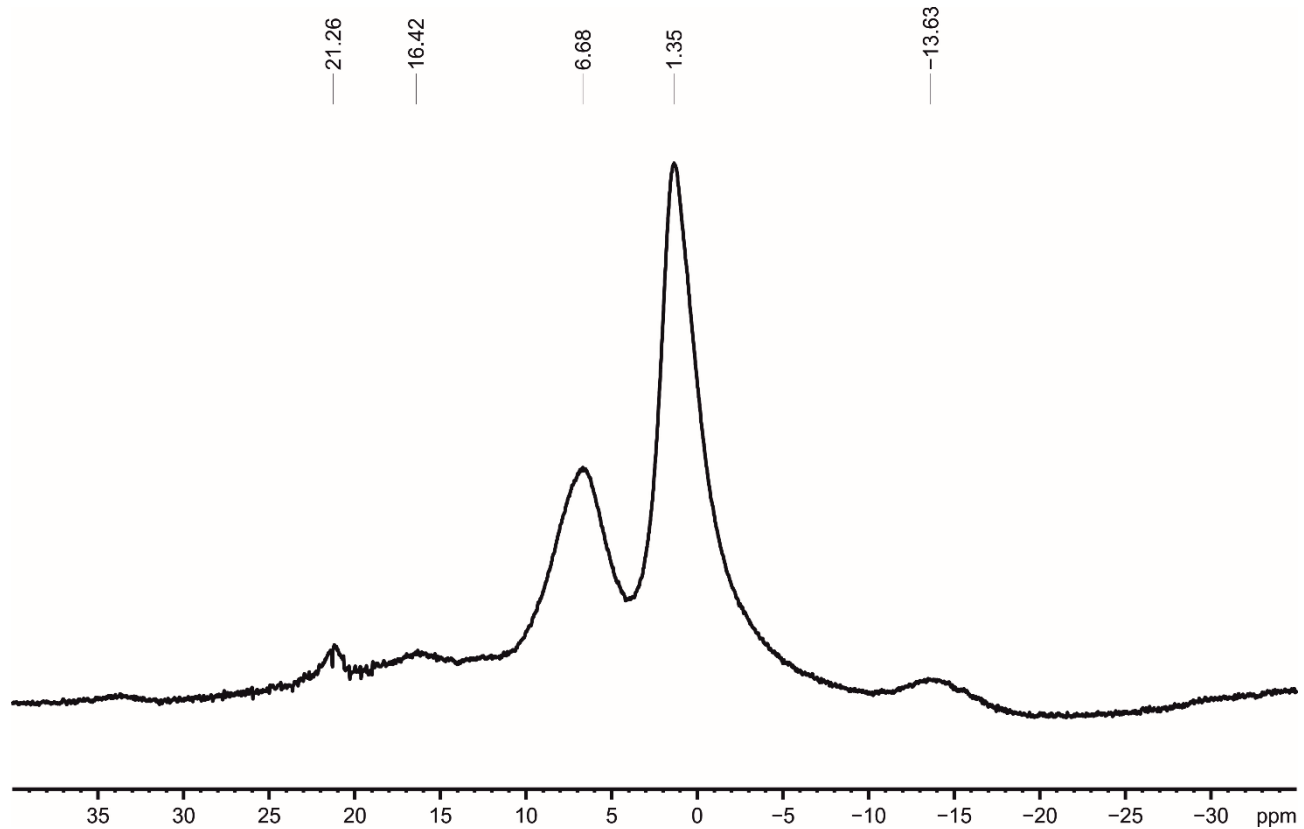


Fig. S2. ¹H MAS NMR spectrum of **1@2a**.

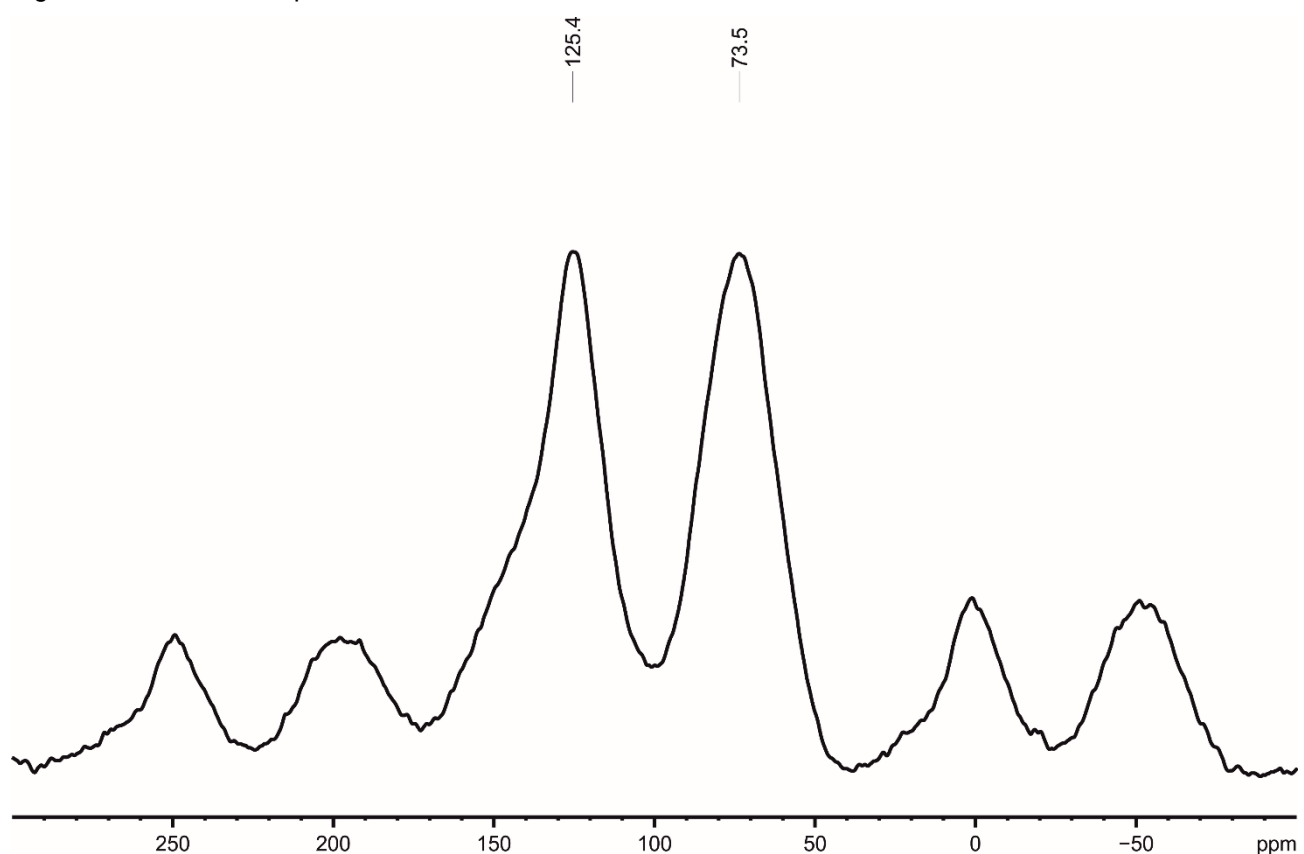


Fig. S3. ¹³P{¹H} MAS NMR spectrum of **1@2a**.

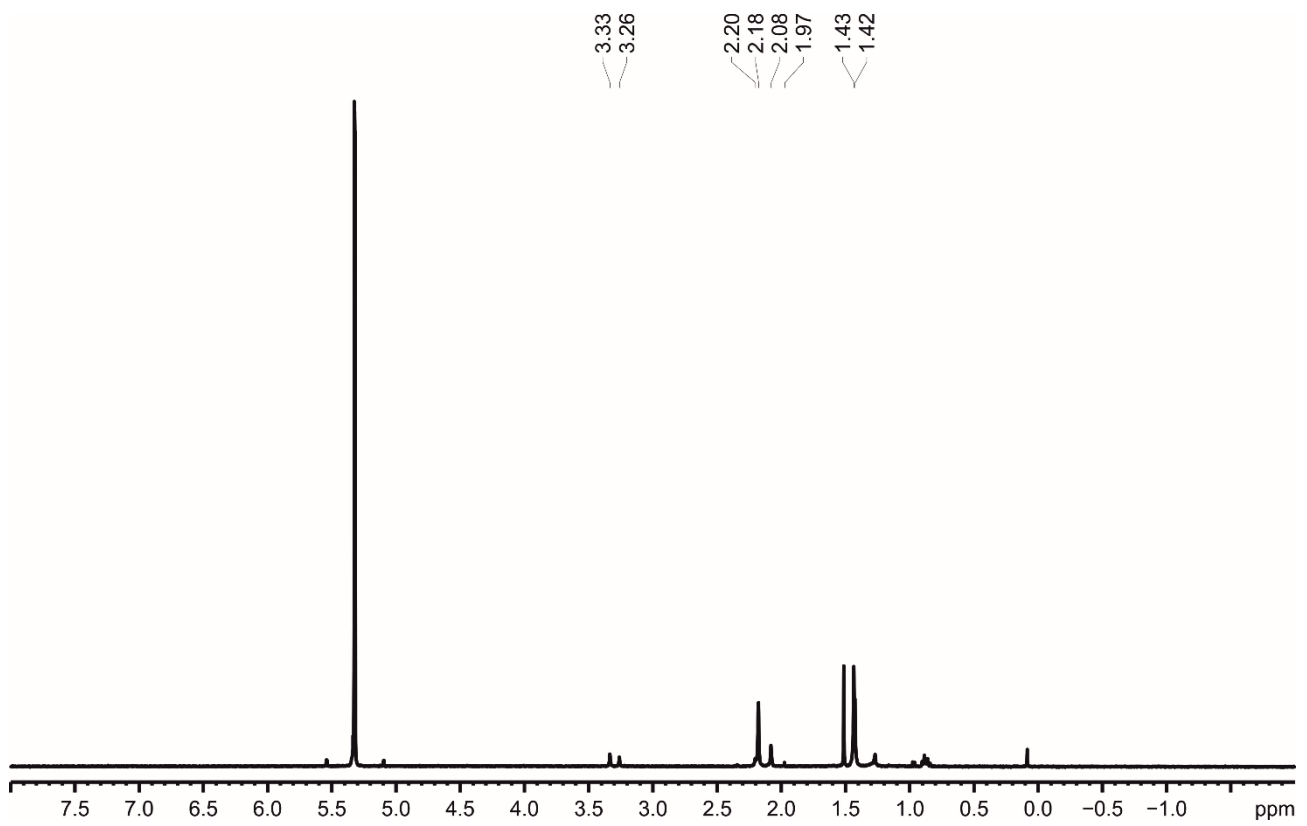


Fig. S4. ¹H NMR spectrum of **1@2a** in CD₂Cl₂.

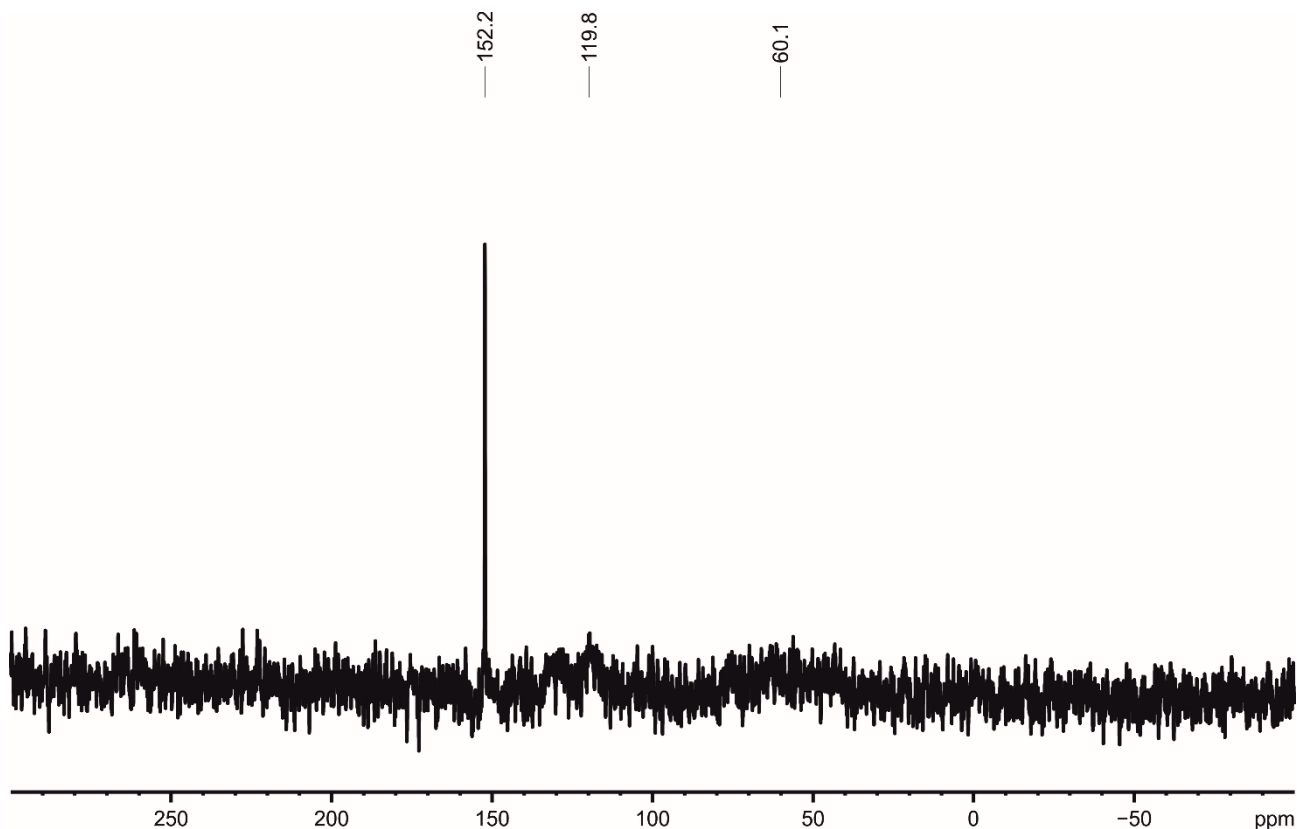


Fig. S5. ³¹P{¹H} NMR spectrum of **1@2a** in CD₂Cl₂.

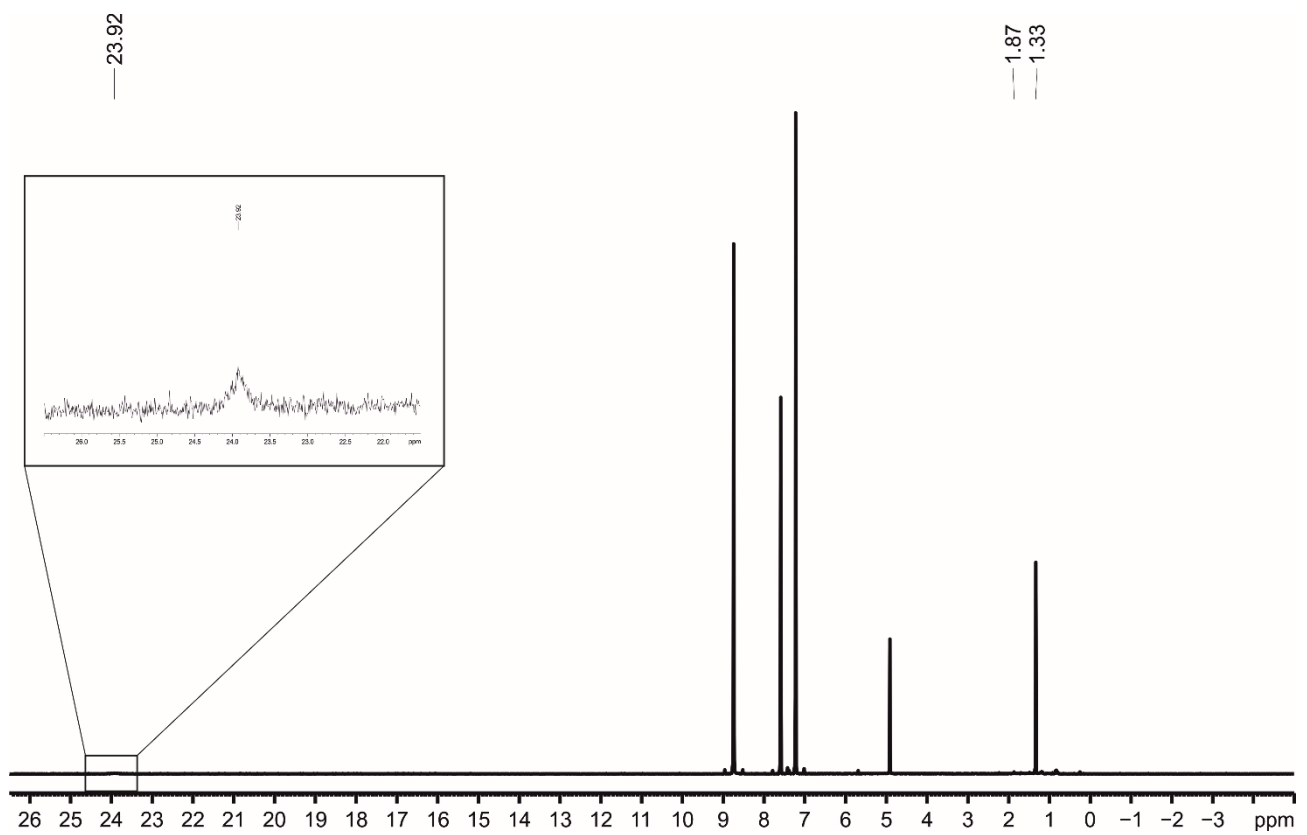


Fig. S6. ^1H NMR spectrum of **1@2a** in pyridine- d_5 .

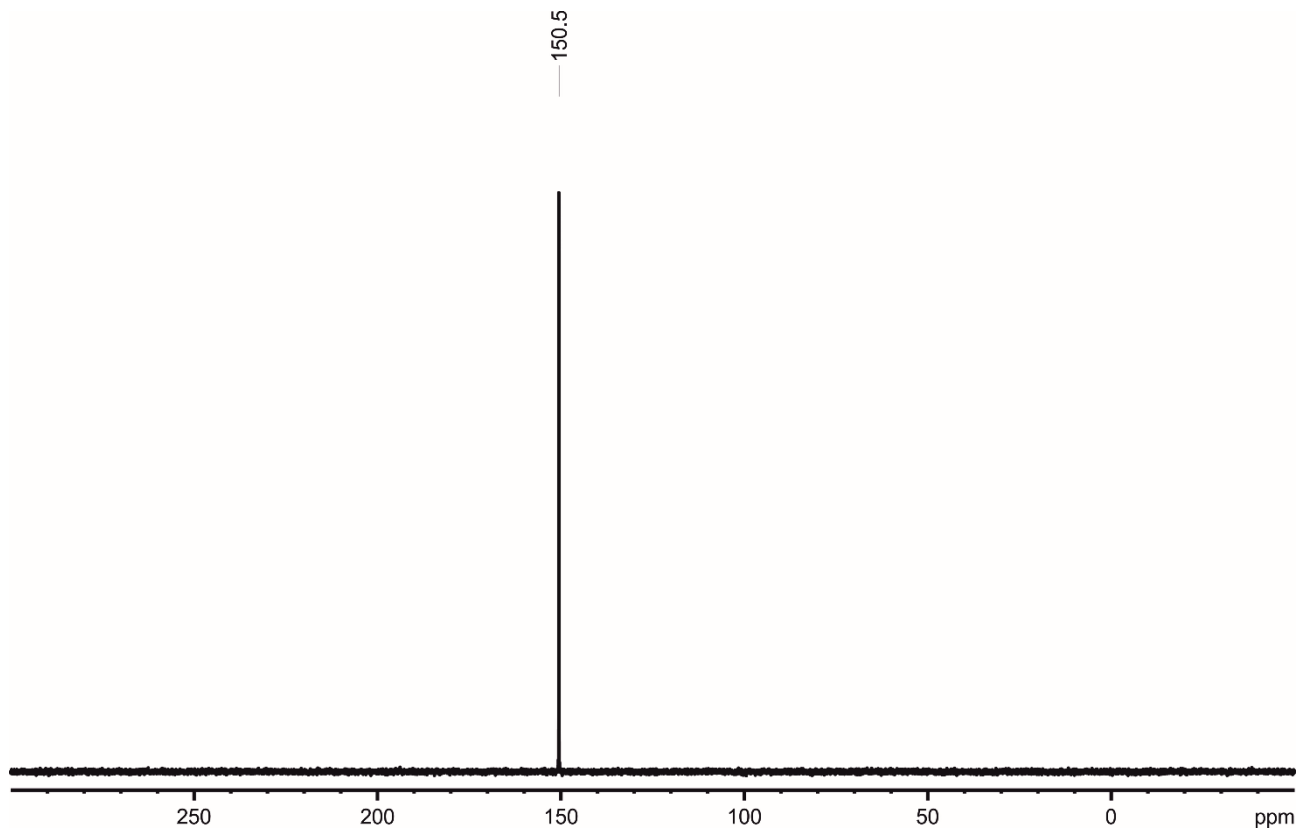


Fig. S7. $^{31}\text{P}\{\text{H}\}$ NMR spectrum of **1@2a** in pyridine- d_5 .

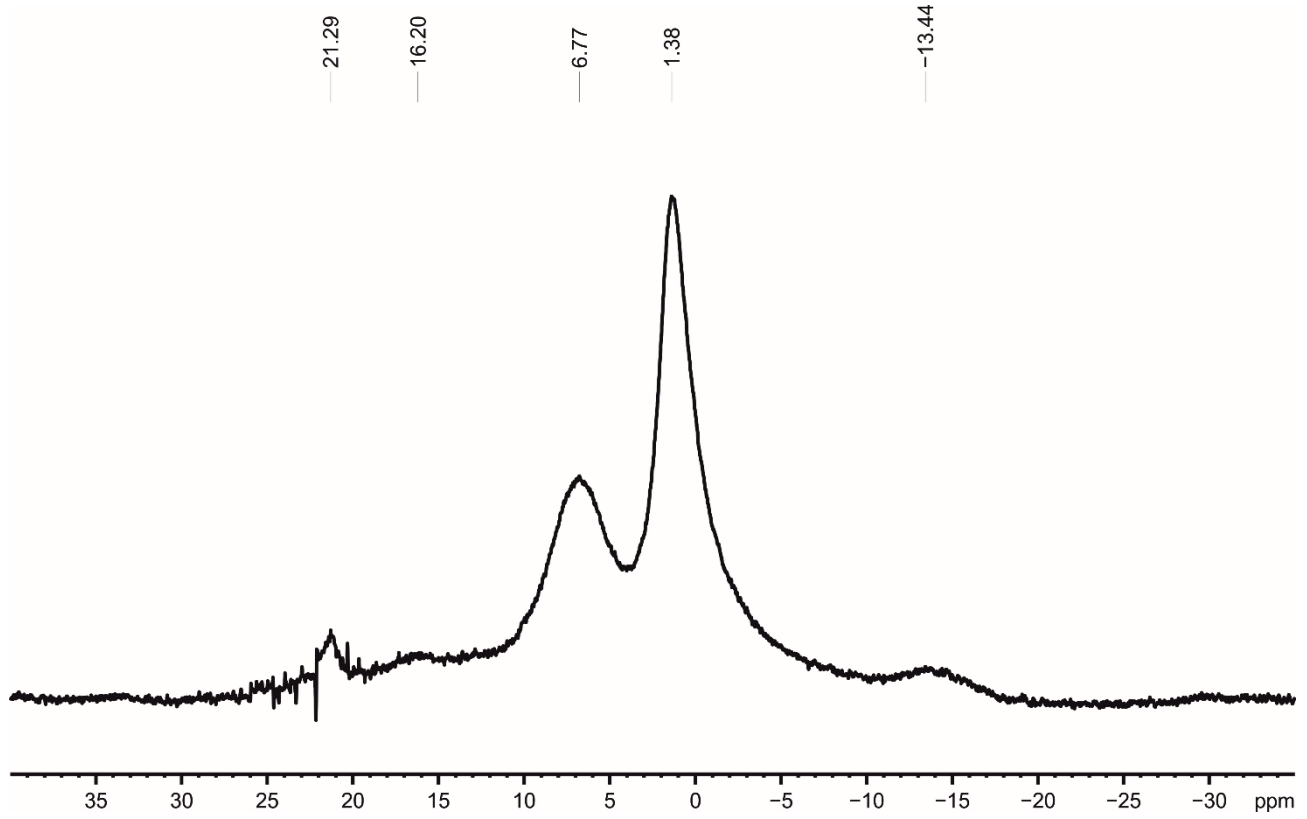


Fig. S8. ¹H MAS NMR spectrum of **1@2b**.

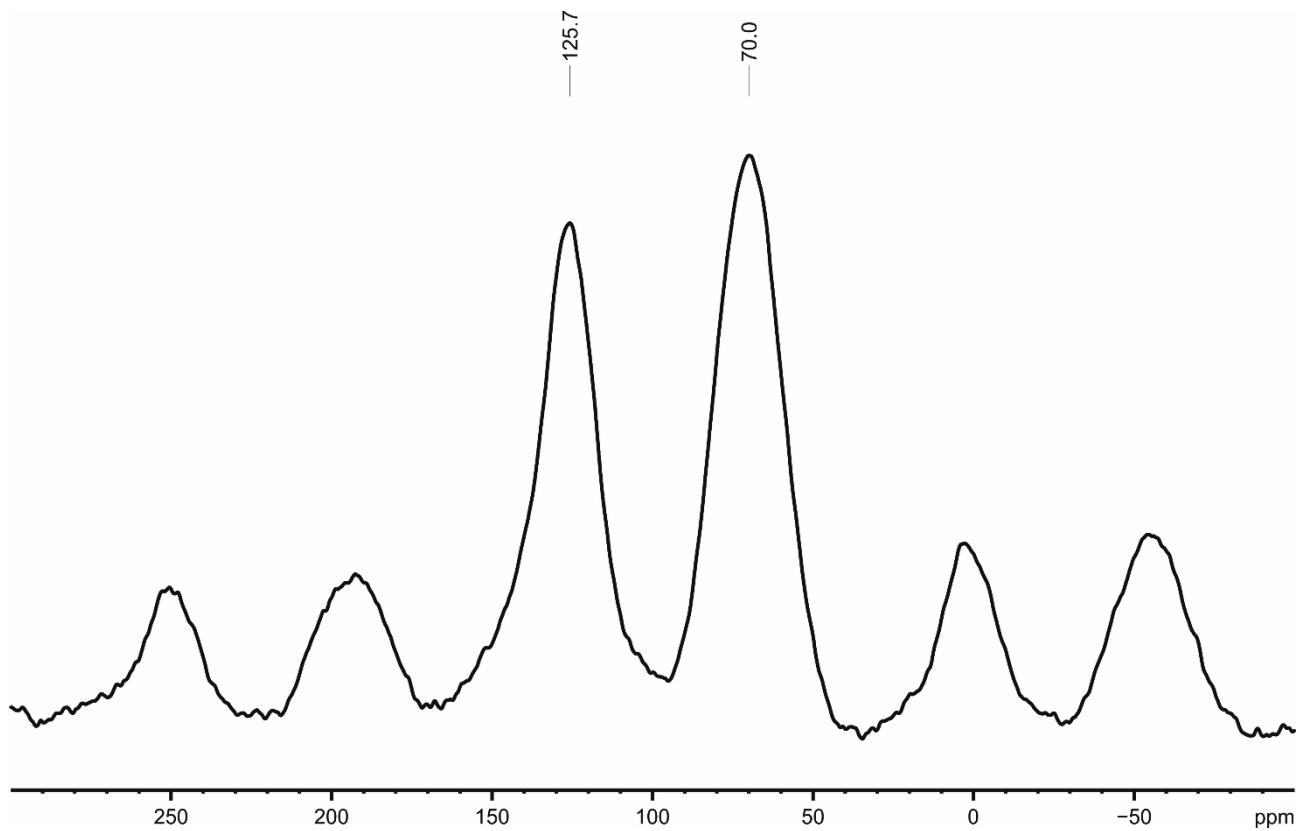


Fig. S9. ³¹P{¹H} MAS NMR spectrum of **1@2b**.

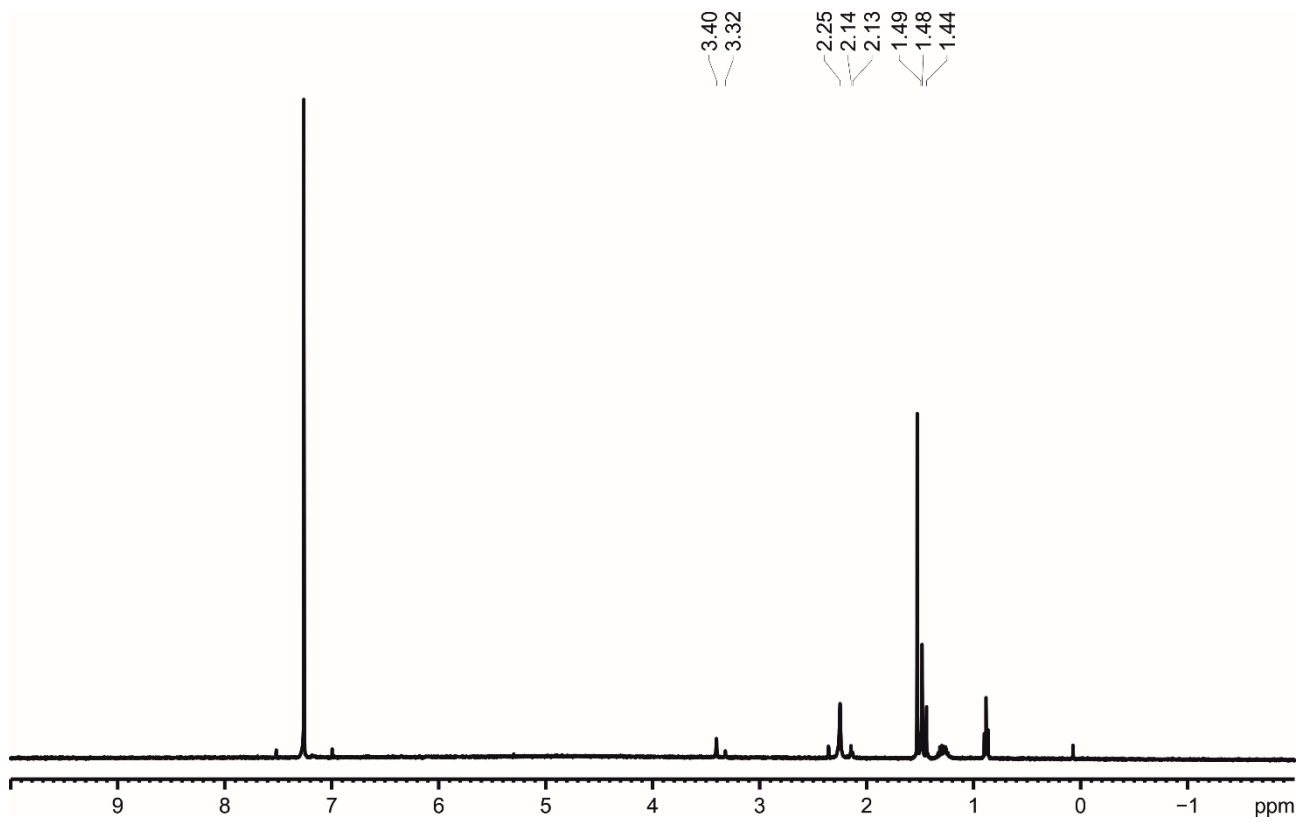


Fig. S10. ^1H NMR spectrum of **1@2b** in CDCl_3 .

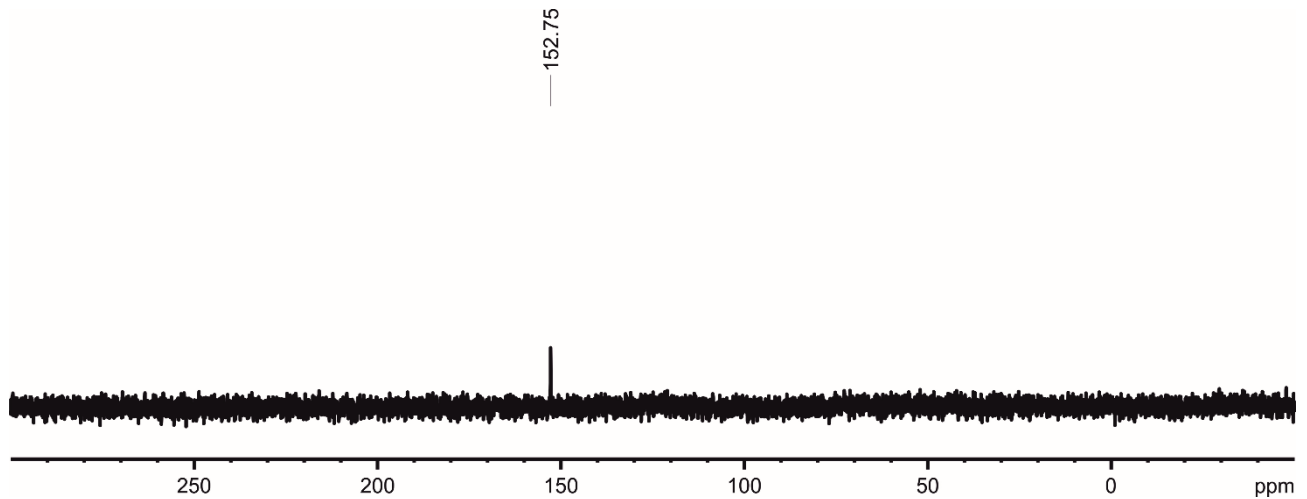


Fig. S11. $^{31}\text{P}\{^1\text{H}\}$ NMR spectrum of **1@2b** in CDCl_3 .

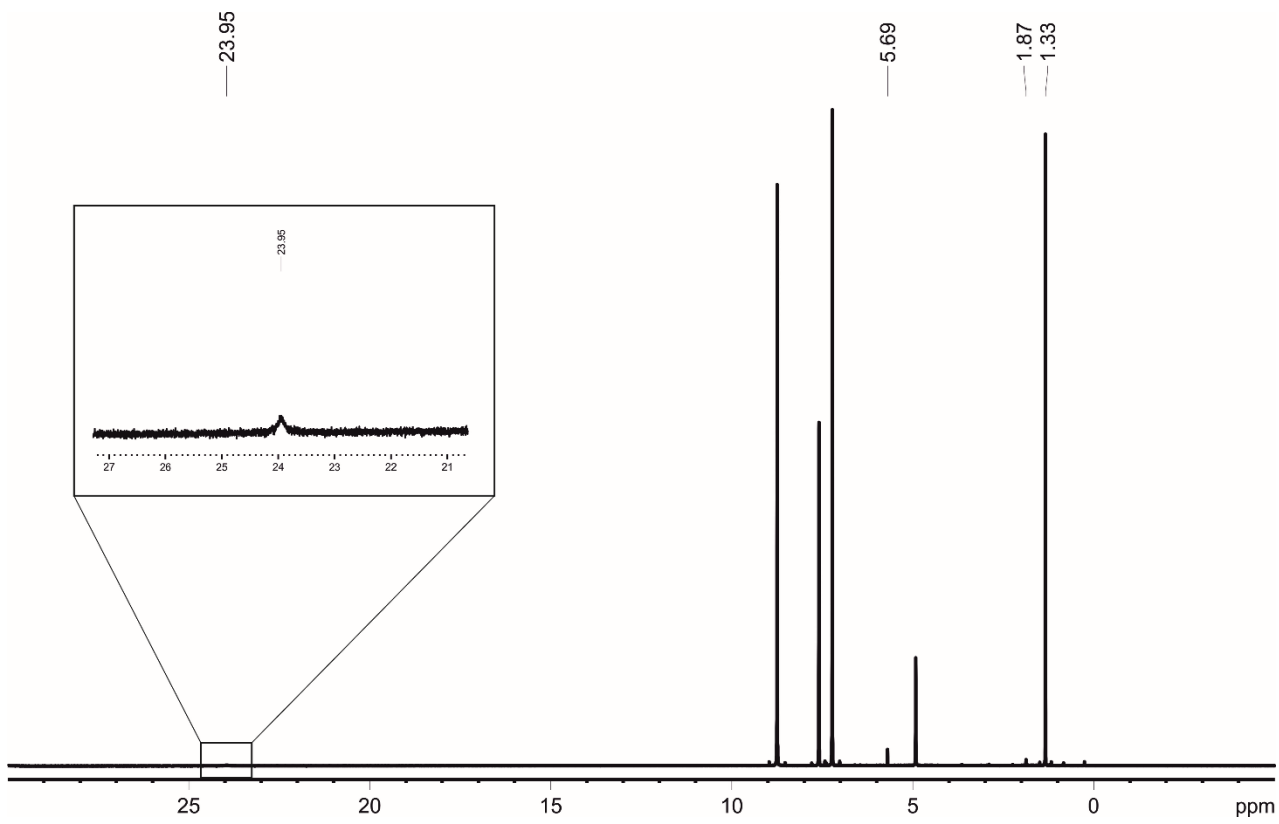


Fig. S12. ^1H NMR spectrum of **1@2b** in pyridine- d_5 .

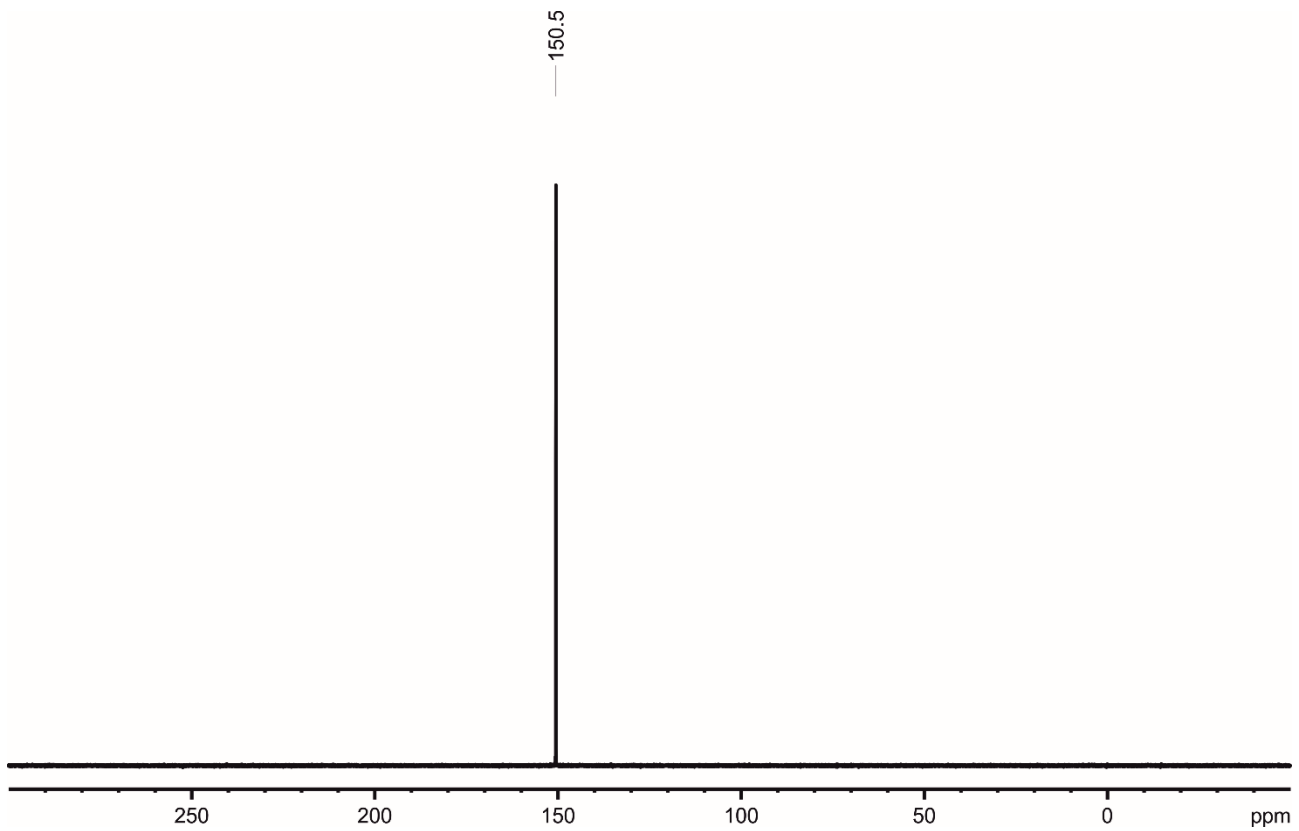


Fig. S13. $^{31}\text{P}\{^1\text{H}\}$ NMR spectrum of **1@2b** in pyridine- d_5 .

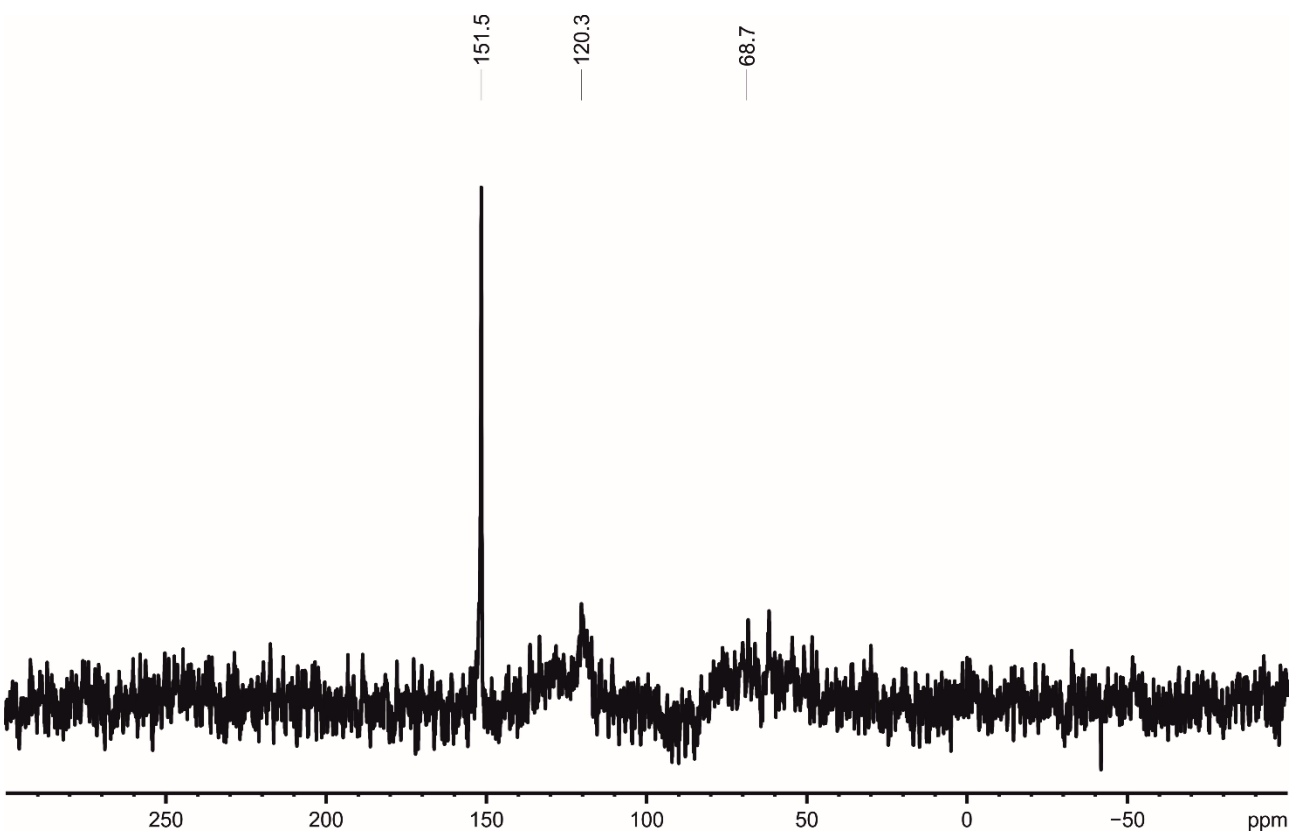
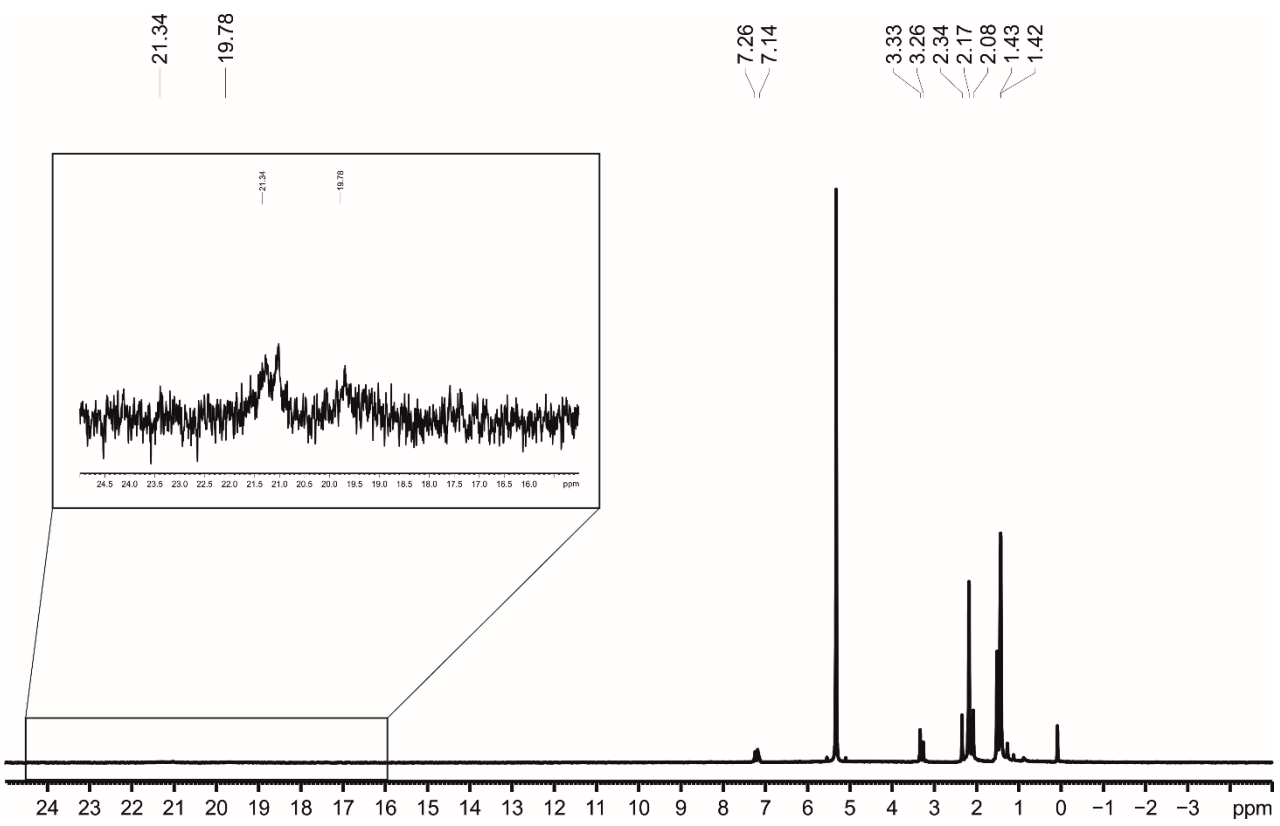


Fig. S15. $^{31}\text{P}\{^1\text{H}\}$ NMR spectrum of $[\text{CpCr}(\mu,\eta^5\text{-As}_5)]@\text{B}$ in CD_2Cl_2 .

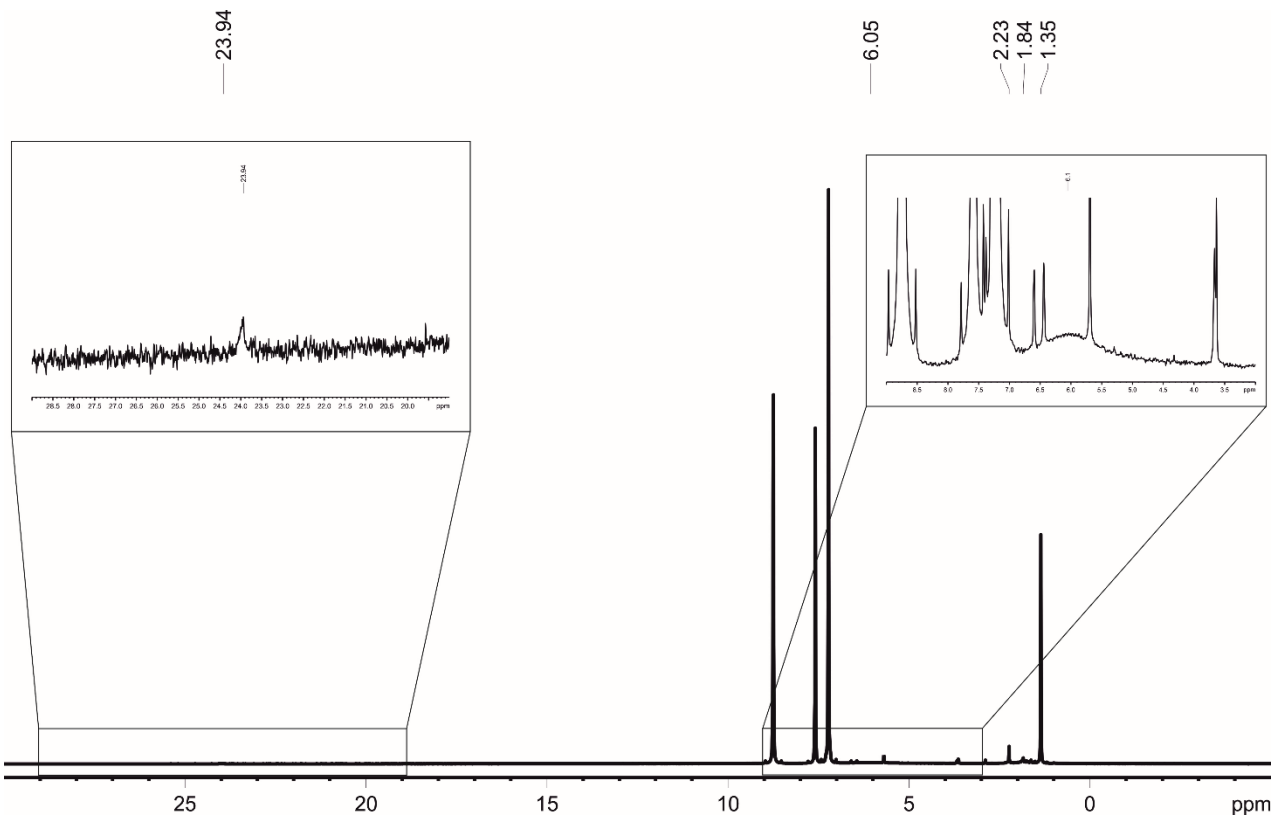


Fig. S16. ^1H NMR spectrum of $[\text{CpCr}(\mu,\eta^5\text{-As}_5)]@\text{B}$ in pyridine- d_5 .

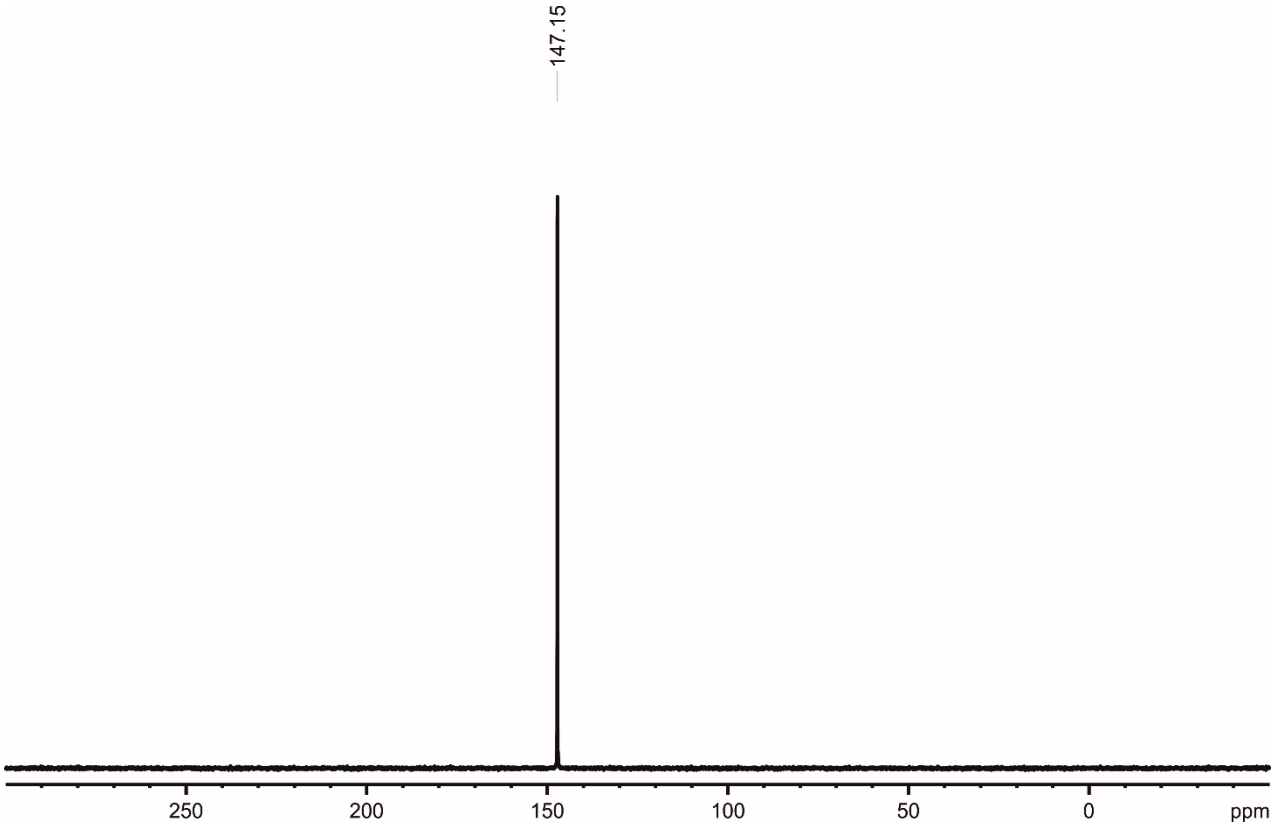


Fig. S17. $^{31}\text{P}\{^1\text{H}\}$ NMR spectrum of $[\text{CpCr}(\mu,\eta^5\text{-As}_5)]@\text{B}$ in pyridine- d_5 .

3 Crystallographic Details

Crystals of **1** and **1@2a** and **1@2b** were taken from a Schlenk flask under a stream of argon and immediately covered with mineral oil (**1**) or perfluorinated Fomblin® mineral oil (**1@2a**, **1@2b**) to prevent both decomposition and a loss of solvent. The quickly chosen single crystals covered by a thin layer of the oil were taken to the pre-centered goniometer head with suitable CryoMount® and directly attached to the goniometer into a stream of cold nitrogen. The X-ray diffraction study of **2a** and **2b** faced many challenges, since the crystals were systematically twinned by merohedry and quickly decomposed due to the loss of solvent. Due to the low diffraction power of **1@2a** and **1@2b** at high theta angles the collection of data required high exposure times.

The data for **1** and **1@2a** were collected using 1° (**1**) or 0.5° (**1@2a**) ω scans on a Rigaku Oxford Diffraction diffractometer equipped with a Titan^{S2} CCD detector and a SuperNova CuK α microfocus source. The data for **1@2b** were collected at P11 beamline of PETRA III (DESY, Hamburg) using 20 keV synchrotron radiation ($\lambda = 0.6199 \text{ \AA}$) and scan width 0.3 deg. The measurements of **1** and **2a** were performed at 123 K, the experiment for **1@2b** was performed at 80 K.

The data processing and reduction was performed with CrysAlisPRO Software.^[3] The structures were solved by direct methods with *SHELX97* and refined by full-matrix least-squares method on $|F|^2$ using multiprocessor and variable memory version *SHELXL2014*.^[4] All ordered non-hydrogen atoms were refined in an anisotropic approximation, while the disordered atoms with occupancy factors less than 0.5 were refined isotropically. The hydrogen atoms were refined as riding on pivot atoms. Crystallographic data and details of the diffraction experiments are given in Table S1, bond lengths and angles are listed in Tables S2-S4, and molecular structures **1**, **1@2** are depicted in Figs.S18-S21.

CIF files with comprehensive information on the details of the diffraction experiments and full tables of bond lengths and angles for **1**, **1@2a** and **1@2b** are deposited in Cambridge Crystallographic Data Centre under the deposition codes CCDC-1875092, CCDC-1875093 and CCDC-1875094, respectively.

Table S1 Experimental details for compounds **1, **1@2a** and **1@2b****

Crystal Data	1	1@2a	1@2b
CCDC-Code	CCDC 1875092	CCDC 1875093	CCDC 1875094
Chemical formula	C ₁₀ H ₁₀ As ₅ Cr ₂	C ₁₁₀ H ₁₆₅ Cl _{13.35} Cu _{13.35} Fe ₁₁ P ₅₅ ·C ₁₀ H ₁₀ As ₅ Cr ₂ ·2.96(CH ₂ Cl ₂)·3.825(CH ₃ CN)	C ₁₁₀ H ₁₆₅ Br _{14.55} Cu _{14.55} Fe ₁₁ P ₅₅ ·C ₁₀ H ₁₀ As ₅ Cr ₂ ·3.4(CH ₂ Cl ₂)·0.9(CH ₃ CN)
M _r	608.78	6143.82	6826.78
Crystal system, space group	Monoclinic, P2 ₁ /n	Monoclinic, Cc	Monoclinic, Cc
Temperature (K)	123	123(2)	80
a, b, c (Å)	8.1149(2), 14.8158(3), 12.0097(3)	30.4118(4), 29.4289(2), 28.8188(3)	27.08802(13), 33.62013(12), 25.36593(11)
β (°)	104.644(3)	112.8746(13)	103.3511(5)
V (Å ³)	1397.00(6)	23764.1(4)	22476.47(17)
Z	4	4	4
F(000)	1132	12166	13251
D _x (Mg m ⁻³)	2.895	1.717	2.017
Radiation type	Cu K α	Cu K α	Synchrotron, $\lambda = 0.6199 \text{ \AA}$
μ (mm ⁻¹)	25.87	13.74	4.11
Crystal color and shape	Black rod	brown rod	brown rod
Crystal size (mm)	0.32 × 0.12 × 0.10	0.19 × 0.06 × 0.04	0.15 × 0.07 × 0.05
Data collection			
Diffractometer	SuperNova, Titan ^{S2}	SuperNova, Titan ^{S2}	P11 beamline, PETRA III, DESY, Dectris PILATUS 6M
Absorption correction	Gaussian	Gaussian	Multi-scan
T _{min} , T _{max}	0.047, 0.306	0.239, 0.651	0.868, 1.000
No. of measured, independent and observed [$I > 2\sigma(I)$] reflections	4560, 2677, 2404	83809, 31629, 26711	256480, 81091, 64928
R _{int}	0.071	0.109	0.045
(sin θ/λ) _{max} (Å ⁻¹)	0.624	0.624	0.845
Range of h, k, l	$h = -8 \rightarrow 10, k = -17 \rightarrow 17, l = -9 \rightarrow 14$	$h = -23 \rightarrow 37, k = -35 \rightarrow 35, l = -35 \rightarrow 34$	$h = -44 \rightarrow 45, k = -49 \rightarrow 49, l = -41 \rightarrow 42$
Refinement			
R[$F^2 > 2\sigma(F^2)$], wR(F^2), S	0.071, 0.205, 1.08	0.056, 0.144, 1.01	0.039, 0.107, 0.96
No. of reflections	2677	31627	81064
No. of parameters	154	2341	2260
No. of restraints	0	117	12
H-atom treatment	H-atom parameters constrained	H atom parameters constrained	H-atom parameters constrained
Δρ _{max} , Δρ _{min} (e Å ⁻³)	2.33, -1.97	1.51, -1.32	2.02, -1.26
Absolute structure	-	Refined as an inversion twin	Refined as an inversion twin

Computer programs: *CrysAlis PRO* 1.171.38.46 and 1.171.38.37b (Rigaku OD, 2015), *SHELXL97* (Sheldrick, 1998), *SHELXL2014/7* (Sheldrick, 2014).

Crystal structure of **1**

The crystal structure of triple decker complex **1** in the solid state was not reported so far despite the fact that its synthesis is known since 1989.^[1] According to our observations, the crystals form bunches of small needles and as a result, showed systematic twinning. This is most likely the reason for the lack of this information in the literature. In this work, we could find a crystal suitable for X-ray structure analysis. The triple decker complex **1** lies in a general position of the monoclinic space group $P2_1/n$. In the crystal structure the molecules form pairs connected by As···As van der Waals contacts (Fig. S18). These pairs are packed in a herringbone mode (Fig. S19). Selected geometric parameters are listed in Table S2.

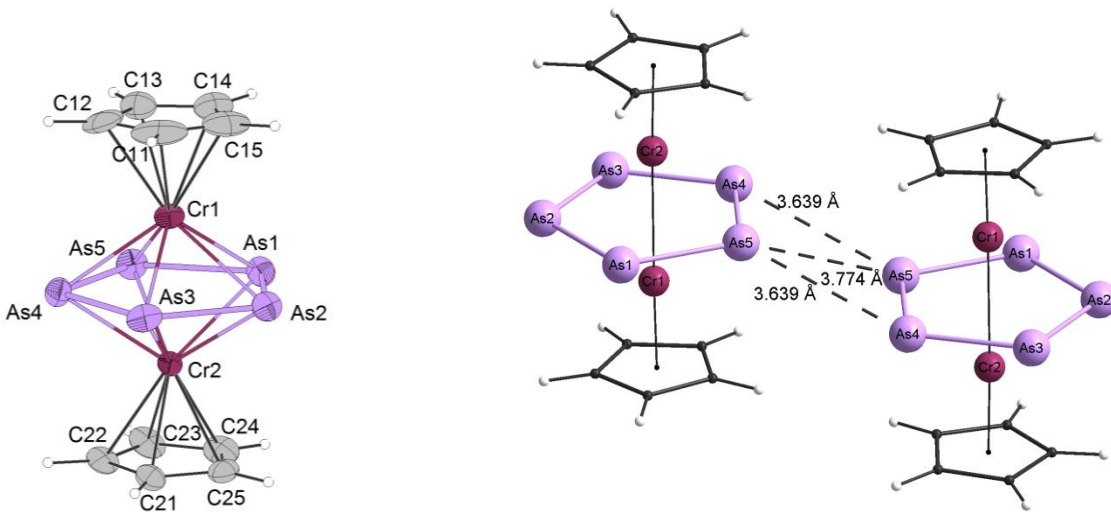


Fig. S18. Molecular structure of $[(\text{CpCr})_2\text{As}_5]$ (**1**), (left) (ellipsoids at 50% probability); (right) pair of molecules with As···As van der Waals contacts (dashed lines, 3.64 – 3.77 Å) in the crystal structure of **1**.

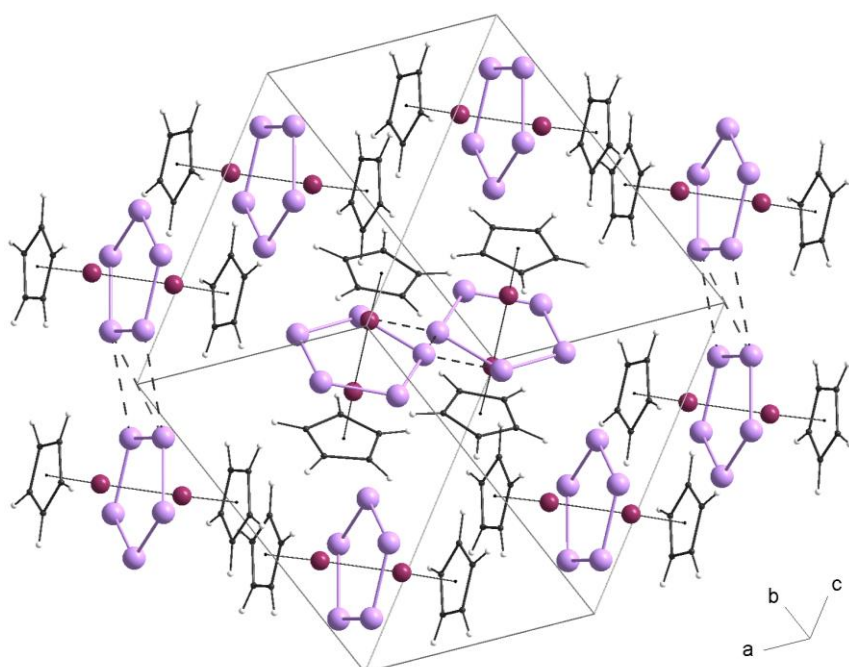


Fig. S19. Crystal packing in the structure of $[(\text{CpCr})_2\text{As}_5]$. The shortest As···As van der Waals contacts are shown by dashed lines.

Table S2. Selected geometric parameters of 1

As5—Cr1	2.4502 (14)	Cr2—C25	2.200 (8)
As5—Cr2	2.4663 (14)	Cr2—C22	2.201 (8)
As3—Cr2	2.4692 (14)	Cr2—Cr1	2.7791 (18)
As3—Cr1	2.4929 (13)	Cr1—C13	2.187 (9)
As1—Cr1	2.4114 (15)	Cr1—C12	2.196 (9)
As1—Cr2	2.4425 (13)	Cr1—C15	2.196 (10)
As4—Cr1	2.5062 (15)	Cr1—C14	2.200 (9)
As4—Cr2	2.5235 (16)	Cr1—C11	2.205 (9)
As2—Cr2	2.4131 (13)	C21—C25	1.419 (14)
As2—Cr1	2.4976 (16)	C21—C22	1.422 (12)
As3—As2	2.5241 (16)	C22—C23	1.424 (14)
As3—As4	2.4698 (17)	C25—C24	1.410 (13)
As5—As1	2.4795 (16)	C13—C14	1.393 (15)
As5—As4	2.5144 (15)	C13—C12	1.410 (14)
As1—As2	2.5476 (16)	C24—C23	1.420 (14)
Cr2—C23	2.186 (8)	C14—C15	1.418 (13)
Cr2—C21	2.198 (8)	C15—C11	1.38 (2)
Cr2—C24	2.198 (9)	C12—C11	1.444 (17)
<hr/>			
As1—As5—As4	107.16 (4)	As3—As4—As5	107.06 (5)
As2—As3—As4	108.42 (5)	As3—As2—As1	109.22 (5)
As2—As1—As5	108.10 (5)		

Crystal structure of compounds **2a** and **2b**

The crystal structures of $[(\text{CpCr})_2\text{As}_5]@[(\text{Cp}^*\text{FeP}_5)_{11}(\text{CuCl})_{13.35}] \cdot 2.96\text{CH}_2\text{Cl}_2 \cdot 3.825\text{MeCN}$ (**2a**) and $[(\text{CpCr})_2\text{As}_5]@[(\text{Cp}^*\text{FeP}_5)_{11}(\text{CuBr})_{14.55}] \cdot 3.4(\text{CH}_2\text{Cl}_2) \cdot 0.9\text{MeCN}$ (**2b**) relate to the different structural types in the same polar Cc space group (Table S1). Despite many attempts made to find a single crystal, both crystals are slightly twinned by merohedry. Therefore the twin model was applied during structure refinement and resulted in some improvement of the quality factors for **2a**. In the case of **2b**, no significant improvement was observed since the anomalous effect is very weak at short wavelengths (Table S1). In the case of **2a**, measured using softer X-rays, the anomalous effect is higher giving more reliable results on the twinning components. The twin batches were refined as 0.957(5)/0.043(5) and 0.958(4)/0.042(4) for **2a** and **2b**, respectively.

A supramolecule **2** occupies a general position of the Cc space group in both structures (Fig. S20, S21). Some positions of the CuX fragments opposite to the bottleneck (resulting in, so to say, a ‘leaking bowl’) are partly vacant indicated by enlarged displacement parameters of corresponding atoms. The occupancies for these positions were refined with fixed isotropic U_{iso} similar to average $U_{\text{iso}} = 0.035 \text{\AA}^{-2}$ for the fully occupied heavy atoms in the corresponding structure. The constraints on the Cu and Br displacement parameters were then removed and refined in an anisotropic approximation.

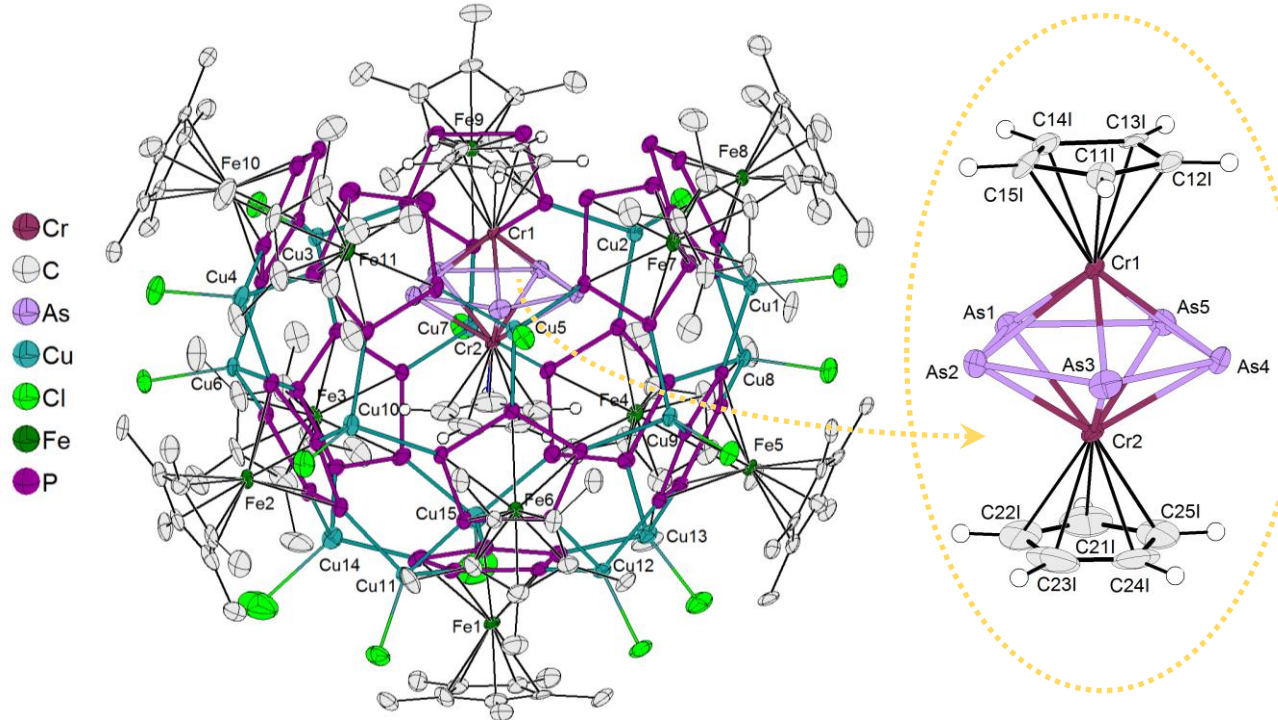


Fig. S20. Molecular structure of (left) supramolecule **1@2a** (ellipsoids at 50% probability). Hydrogen atoms are hidden for clarity; (right) encapsulated guest molecule $[(\text{CpCr})_2\text{As}_5]$ with enumeration scheme (cf. Tables S2, S3).

Table S3. Selected geometric parameters of 2a

Cr1—C14I	2.188 (11)	Fe2—P25	2.343 (3)
Cr1—C15I	2.195 (12)	Fe2—P21	2.384 (3)
Cr1—C11I	2.198 (11)	Fe2—P23	2.388 (3)
Cr1—C12I	2.207 (11)	Fe3—P33	2.344 (3)
Cr1—C13I	2.210 (10)	Fe3—P31	2.359 (3)
Cr1—As1	2.474 (2)	Fe3—P35	2.363 (4)
Cr1—As5	2.480 (2)	Fe3—P32	2.363 (3)
Cr1—As4	2.499 (2)	Fe3—P34	2.375 (4)
Cr1—As2	2.5008 (19)	Fe4—P44	2.356 (3)
Cr1—As3	2.515 (2)	Fe4—P42	2.358 (3)
Cr1—Cr2	2.740 (2)	Fe4—P43	2.365 (4)
C11I—C15I	1.416 (15)	Fe4—P41	2.366 (3)
C11I—C12I	1.426 (17)	Fe4—P45	2.396 (3)
C12I—C13I	1.443 (15)	Fe5—P51	2.347 (3)
C13I—C14I	1.417 (15)	Fe5—P53	2.348 (3)
C14I—C15I	1.417 (16)	Fe5—P54	2.359 (3)
Cr2—C25I	2.147 (16)	Fe5—P52	2.374 (3)
Cr2—C24I	2.175 (14)	Fe5—P55	2.390 (3)
Cr2—C21I	2.175 (14)	Fe6—P64	2.334 (3)
Cr2—C22I	2.182 (14)	Fe6—P65	2.345 (3)
Cr2—C23I	2.190 (14)	Fe6—P62	2.351 (3)
Cr2—As1	2.468 (2)	Fe6—P61	2.353 (3)
Cr2—As5	2.4789 (19)	Fe6—P63	2.386 (3)
Cr2—As2	2.508 (2)	Fe7—P74	2.331 (3)
Cr2—As4	2.508 (2)	Fe7—P72	2.366 (3)
Cr2—As3	2.533 (2)	Fe7—P75	2.367 (3)
As1—As2	2.4729 (17)	Fe7—P71	2.380 (3)
As1—As5	2.4847 (17)	Fe7—P73	2.382 (3)
As2—As3	2.4249 (18)	Fe8—P83	2.343 (3)
As3—As4	2.4260 (17)	Fe8—P84	2.346 (3)

As4—As5	2.4558 (17)	Fe8—P82	2.364 (3)
C21I—C22I	1.34 (3)	Fe8—P85	2.366 (3)
C21I—C25I	1.38 (3)	Fe8—P81	2.377 (3)
C22I—C23I	1.46 (3)	Fe9—P95	2.336 (3)
C23I—C24I	1.34 (3)	Fe9—P93	2.342 (3)
C24I—C25I	1.40 (3)	Fe9—P94	2.350 (3)
Cu1—Cl1	2.210 (3)	Fe9—P91	2.367 (3)
Cu1—P82	2.293 (3)	Fe9—P92	2.374 (3)
Cu1—P73	2.306 (3)	Fe10—P105	2.339 (4)
Cu1—P55	2.306 (3)	Fe10—P101	2.350 (3)
Cu2—Cl2	2.218 (3)	Fe10—P104	2.356 (3)
Cu2—P95	2.303 (3)	Fe10—P102	2.367 (3)
Cu2—P84	2.307 (3)	Fe10—P103	2.375 (3)
Cu2—P43	2.314 (3)	Fe11—P115	2.337 (4)
Cu3—Cl3	2.221 (3)	Fe11—P114	2.365 (3)
Cu3—P93	2.289 (3)	Fe11—P113	2.371 (3)
Cu3—P101	2.306 (3)	Fe11—P111	2.372 (3)
Cu3—P32	2.310 (3)	Fe11—P112	2.377 (4)
Cu4—Cl4	2.216 (3)	P11—P15	2.099 (4)
Cu4—P21	2.319 (4)	P11—P12	2.105 (4)
Cu4—P111	2.321 (3)	P12—P13	2.108 (4)
Cu4—P104	2.322 (3)	P13—P14	2.107 (4)
Cu5—Cl5	2.226 (3)	P14—P15	2.099 (4)
Cu5—P114	2.313 (3)	P21—P25	2.101 (4)
Cu5—P75	2.324 (3)	P21—P22	2.107 (4)
Cu5—P63	2.334 (3)	P22—P23	2.110 (4)
Cu6—Cl6	2.205 (3)	P23—P24	2.107 (4)
Cu6—P22	2.281 (3)	P24—P25	2.112 (4)
Cu6—P105	2.298 (3)	P31—P35	2.099 (5)
Cu6—P31	2.300 (3)	P31—P32	2.099 (4)
Cu7—Cl7	2.222 (3)	P32—P33	2.112 (4)
Cu7—P33	2.313 (3)	P33—P34	2.104 (4)
Cu7—P44	2.317 (3)	P34—P35	2.127 (4)
Cu7—P94	2.320 (3)	P41—P45	2.107 (4)
Cu8—Cl8	2.212 (3)	P41—P42	2.117 (4)
Cu8—P42	2.302 (3)	P42—P43	2.098 (4)
Cu8—P51	2.303 (3)	P43—P44	2.102 (4)
Cu8—P83	2.309 (4)	P44—P45	2.118 (4)
Cu9—Cl9	2.222 (3)	P51—P55	2.102 (4)
Cu9—P64	2.293 (3)	P51—P52	2.111 (4)
Cu9—P54	2.298 (3)	P52—P53	2.107 (4)
Cu9—P74	2.299 (3)	P53—P54	2.108 (4)
Cu10—Cl10	2.214 (3)	P54—P55	2.099 (4)
Cu10—P25	2.292 (3)	P61—P65	2.102 (4)
Cu10—P62	2.293 (3)	P61—P62	2.107 (4)
Cu10—P115	2.303 (4)	P62—P63	2.098 (4)
Cu11—Cl11	2.206 (3)	P63—P64	2.096 (4)
Cu11—P24	2.292 (3)	P64—P65	2.102 (4)
Cu11—P61	2.310 (3)	P71—P75	2.109 (4)
Cu11—P11	2.312 (3)	P71—P72	2.121 (4)
Cu12—Cl12	2.201 (3)	P72—P73	2.104 (5)
Cu12—P53	2.303 (3)	P73—P74	2.107 (4)
Cu12—P15	2.304 (3)	P74—P75	2.100 (4)
Cu12—P65	2.305 (3)	P81—P82	2.098 (4)
Cu13—Cl13	2.211 (4)	P81—P85	2.115 (4)
Cu13—P14	2.319 (3)	P82—P83	2.104 (4)
Cu13—P52	2.324 (3)	P83—P84	2.096 (4)

Cu13—P41	2.324 (3)	P84—P85	2.107 (5)
Cu14*—P12	2.144 (9)	P91—P95	2.111 (4)
Cu14*—P23	2.299 (10)	P91—P92	2.117 (4)
Cu14*—P35	2.344 (9)	P92—P93	2.110 (4)
Cu14*—Cl14	2.562 (11)	P93—P94	2.106 (4)
Cu15*—P13	2.235 (13)	P94—P95	2.100 (4)
Cu15*—Cl15	2.29 (3)	P101—P105	2.097 (4)
Cu15*—P34	2.296 (14)	P101—P102	2.101 (4)
Cu15*—P45	2.401 (13)	P102—P103	2.126 (4)
Fe1—P15	2.329 (3)	P103—P104	2.101 (4)
Fe1—P11	2.339 (3)	P104—P105	2.104 (4)
Fe1—P14	2.353 (3)	P111—P115	2.103 (4)
Fe1—P12	2.367 (3)	P111—P112	2.112 (5)
Fe1—P13	2.377 (3)	P112—P113	2.115 (4)
Fe2—P24	2.338 (3)	P113—P114	2.107 (5)
Fe2—P22	2.342 (3)	P114—P115	2.115 (4)
As3—As2—As1	108.05(6)	As4—As5—As1	107.14(6)
As2—As3—As4	108.85(6)	As2—As1—As5	107.33(6)
As3—As4—As5	108.63(6)		

*the site occupation factors for atoms Cu14 and Cu15 are 0.2 and 0.15, respectively.

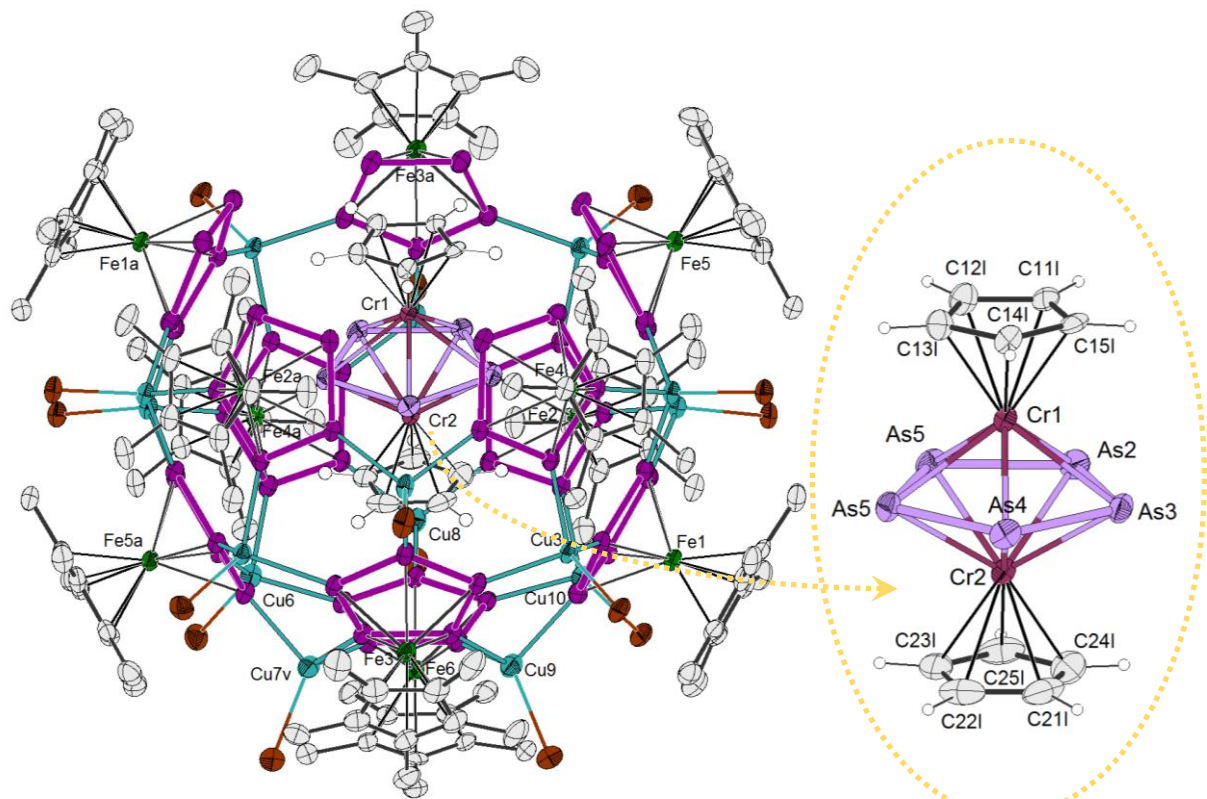


Fig. S21. Molecular structure of (left) supramolecule **1@2b** (ellipsoids at 50% probability). Hydrogen atoms are hidden for clarity; (right) encapsulated guest molecule $[(\text{CpCr})_2\text{As}_5]$ with enumeration scheme (cf. Tables S2, S4).

Table S4. Selected geometric parameters of 2b

Cr1—C13I	2.188 (6)	Fe5—P51	2.3474 (18)
Cr1—C12I	2.191 (6)	Fe5—P55	2.3620 (17)
Cr1—C11I	2.194 (6)	Fe5—P52	2.3629 (17)
Cr1—C14I	2.194 (6)	Fe5—P53	2.3667 (17)
Cr1—C15I	2.203 (6)	Fe5—P54	2.3689 (17)
Cr1—As2	2.4923 (10)	Fe6—P61	2.3486 (17)
Cr1—As3	2.4947 (10)	Fe6—P63	2.3520 (17)
Cr1—As1	2.4956 (10)	Fe6—P62	2.3556 (17)
Cr1—As4	2.5010 (10)	Fe6—P65	2.3573 (17)
Cr1—As5	2.5014 (11)	Fe6—P64	2.3599 (17)
Cr1—Cr2	2.7461 (12)	Fe1A—P14A	2.3431 (17)
Cr2—C21I	2.175 (7)	Fe1A—P15A	2.3667 (17)
Cr2—C24I	2.191 (7)	Fe1A—P11A	2.3733 (17)
Cr2—C22I	2.190 (7)	Fe1A—P13A	2.3732 (16)
Cr2—C25I	2.193 (6)	Fe1A—P12A	2.3755 (17)
Cr2—C23I	2.198 (7)	Fe2A—P24A	2.3458 (17)
Cr2—As2	2.4970 (11)	Fe2A—P25A	2.3502 (16)
Cr2—As1	2.4977 (10)	Fe2A—P22A	2.3639 (17)
Cr2—As3	2.4988 (10)	Fe2A—P23A	2.3643 (18)
Cr2—As4	2.5052 (10)	Fe2A—P21A	2.3752 (16)
Cr2—As5	2.5053 (10)	Fe3A—P32A	2.3428 (19)
As1—As5	2.4518 (9)	Fe3A—P33A	2.3586 (17)
As1—As2	2.4602 (9)	Fe3A—P34A	2.3688 (18)
As2—As3	2.4602 (8)	Fe3A—P31A	2.3714 (19)
As3—As4	2.4505 (8)	Fe3A—P35A	2.3749 (19)
As4—As5	2.4496 (9)	Fe4A—P42A	2.3545 (17)
Cu1—P55	2.3134 (16)	Fe4A—P43A	2.3585 (17)
Cu1—P45	2.3157 (16)	Fe4A—P44A	2.3652 (17)
Cu1—P14	2.3203 (18)	Fe4A—P45A	2.3674 (16)
Cu2—P13	2.3013 (16)	Fe4A—P41A	2.3874 (18)
Cu2—P21	2.3064 (16)	Fe5A—P55A	2.3518 (17)
Cu2—P51	2.3081 (17)	Fe5A—P52A	2.3559 (17)
Cu3—P15	2.2892 (16)	Fe5A—P53A	2.3595 (17)
Cu3—P41	2.2904 (17)	Fe5A—P54A	2.3600 (17)
Cu3—P31	2.2942 (17)	Fe5A—P51A	2.3865 (17)
Cu4—P52A	2.3069 (16)	P11—P15	2.104 (2)
Cu4—P24A	2.3076 (17)	P11—P12	2.109 (2)
Cu4—P33	2.3122 (16)	P11A—P15A	2.110 (2)
Cu5—P25A	2.3047 (16)	P11A—P12A	2.126 (2)
Cu5—P42	2.3110 (17)	P12—P13	2.108 (2)
Cu5—P32	2.3196 (18)	P12A—P13A	2.106 (2)
Cu8—P61	2.3010 (17)	P13—P14	2.104 (2)
Cu8—P23	2.3035 (17)	P13A—P14A	2.106 (2)
Cu8—P43A	2.3171 (16)	P14—P15	2.107 (2)
Cu1A—P55A	2.2974 (16)	P14A—P15A	2.107 (2)
Cu1A—P45A	2.2994 (16)	P21—P24	2.103 (2)
Cu1A—P14A	2.3167 (17)	P21—P22	2.106 (2)
Cu2A—P13A	2.3123 (17)	P21A—P24A	2.103 (2)
Cu2A—P21A	2.3168 (16)	P21A—P22A	2.111 (2)
Cu2A—P51A	2.3267 (16)	P22—P23	2.109 (2)
Cu3A—P31A	2.3027 (17)	P22A—P23A	2.124 (2)
Cu3A—P41A	2.3102 (17)	P23—P25	2.112 (2)
Cu3A—P15A	2.3108 (16)	P23A—P25A	2.105 (2)
Cu4A—P33A	2.3068 (17)	P24—P25	2.106 (2)
Cu4A—P52	2.3077 (16)	P24A—P25A	2.107 (2)
Cu4A—P24	2.3157 (18)	P31—P32	2.097 (2)

Cu5A—P32A	2.3008 (18)	P31—P35	2.109 (2)
Cu5A—P25	2.3020 (16)	P31A—P32A	2.102 (2)
Cu5A—P42A	2.3060 (17)	P31A—P35A	2.108 (2)
Cu6*—P65	2.2941 (17)	P32—P33	2.105 (2)
Cu6*—P44A	2.3009 (18)	P32A—P33A	2.107 (2)
Cu6*—P54A	2.3137 (17)	P33—P34	2.107 (2)
Cu7V*—P64	2.2846 (18)	P33A—P34A	2.107 (2)
Cu7V*—P53A	2.2972 (18)	P34—P35	2.106 (2)
Cu7V*—P34	2.3165 (19)	P34A—P35A	2.118 (2)
Cu9*—P63	2.2744 (18)	P41—P45	2.101 (2)
Cu9*—P35	2.2979 (19)	P41—P42	2.105 (2)
Cu9*—P11	2.3150 (18)	P41A—P45A	2.102 (2)
Cu10*—P62	2.3065 (16)	P41A—P42A	2.103 (2)
Cu10*—P22	2.3174 (17)	P42—P43	2.115 (2)
Cu10*—P12	2.3186 (17)	P42A—P43A	2.105 (2)
Fe1—P13	2.3581 (17)	P43—P44	2.127 (2)
Fe1—P15	2.3630 (17)	P43A—P44A	2.109 (2)
Fe1—P12	2.3696 (17)	P44—P45	2.105 (2)
Fe1—P11	2.3705 (18)	P44A—P45A	2.110 (2)
Fe1—P14	2.3825 (18)	P51—P52	2.106 (2)
Fe2—P23	2.3514 (17)	P51—P55	2.110 (2)
Fe2—P22	2.3547 (17)	P51A—P52A	2.102 (2)
Fe2—P25	2.3575 (16)	P51A—P55A	2.104 (2)
Fe2—P21	2.3660 (16)	P52—P53	2.113 (2)
Fe2—P24	2.3794 (18)	P52A—P53A	2.113 (2)
Fe3—P31	2.3569 (18)	P53—P54	2.121 (2)
Fe3—P33	2.3570 (17)	P53A—P54A	2.112 (2)
Fe3—P34	2.3615 (18)	P54—P55	2.113 (2)
Fe3—P35	2.3659 (19)	P54A—P55A	2.106 (2)
Fe3—P32	2.3777 (19)	P61—P65	2.104 (2)
Fe4—P41	2.3497 (18)	P61—P62	2.105 (2)
Fe4—P42	2.3625 (17)	P62—P63	2.103 (2)
Fe4—P45	2.3663 (16)	P63—P64	2.108 (2)
Fe4—P44	2.3774 (17)	P64—P65	2.105 (2)
Fe4—P43	2.3778 (17)		
As5—As1—As2	108.00(3)	As4—As5—As1	108.10(3)
As3—As2—As1	107.74(3)	As4—As3—As2	108.02(3)
As5—As4—As3	108.14(3)		

*the site occupation factors for atoms Cu6, Cu7v, Cu9 and Cu10 are 0.9, 0.85, 0.9 and 0.9, respectively.

The guest triple decker molecules are ordered in the cavity of the open hosts unlike to the previously reported structure, where the same guest was encapsulated into 90-vertex supramolecule $\{[\text{Cp}^*\text{Fe}(\eta^5\text{-P}_5)]_{12}(\text{CuBr})_{25}(\text{CH}_3\text{CN})_{10}\}$.^[5] The upper deck of the guest slightly protrudes from the open rim of the host and is perfectly complimentary to the shape and size of the ‘bottleneck’ of the host (Fig. S22).

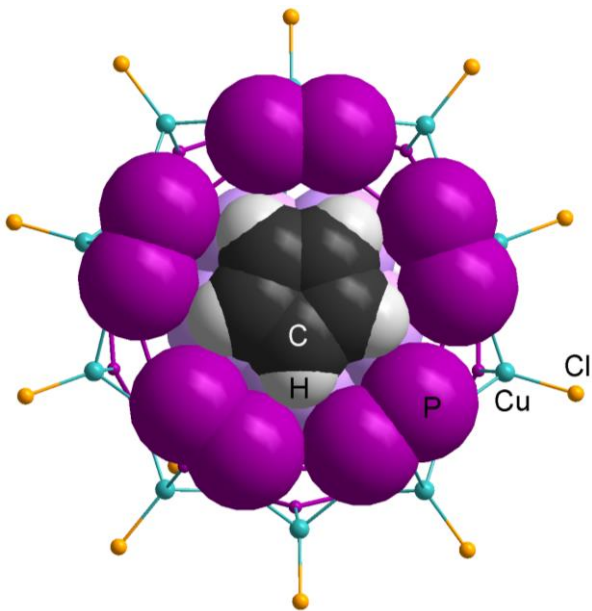


Fig. S22. Exact fit of the guest molecule to a ‘bottleneck’ (view from above) formed by 10 P atoms of 5 *cyclo*-P₅ ligands of the host molecule **1@2a**.

Interestingly, the disordered positions of CH₂Cl₂ solvent molecules are found as complimentary to the positions of the CuX vacancies in the scaffold **1@2** (Fig. S23). Due to the close proximity to the positions of the halogen atoms, a number of geometric restraints have to be applied to refine the solvent molecules. In the interstitial space some CH₂Cl₂ and CH₃CN solvent molecules were located, which are severely disordered. Their occupancies were refined and geometric restraints were used for their refinement. These solvent molecules occupying the vacancies in CuX positions help to stabilize the structural type and increase its stability within a wider range of CuX contents.

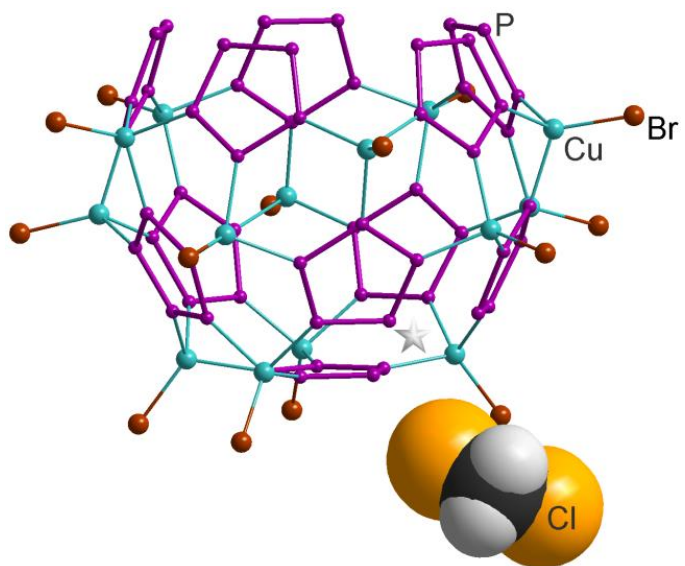


Fig. S23. A ‘leaking bowl’ with a CuX fragment missing (shown as asterisk) at its ‘bottom’ and a CH₂Cl₂ molecule acting as a ‘plug’ in **1@2b**.

4 Solid solutions of supramolecules

Non-integer CuX content in **1@2a** and **1@2b** results from the presence of partly the vacant CuX positions. The overall 13.35 units of CuCl (**1@2a**) and 14.55 of CuBr (**1@2b**) statistically occupy 15 CuX positions. In higher deficient **1@2a**, two vacancies at positions of Cu14 (site occupation factor s.o.f. = 0.20) and Cu15 (s.o.f. = 0.15) are found. In lower deficient **1@2b**, four vacancies at Cu6, Cu7v, Cu9 and Cu10 positions with s.o.f.s 0.90, 0.85, 0.90, 0.90 are found as a result of the s.o.f. refinement, respectively (Fig. S20, S21, S24).

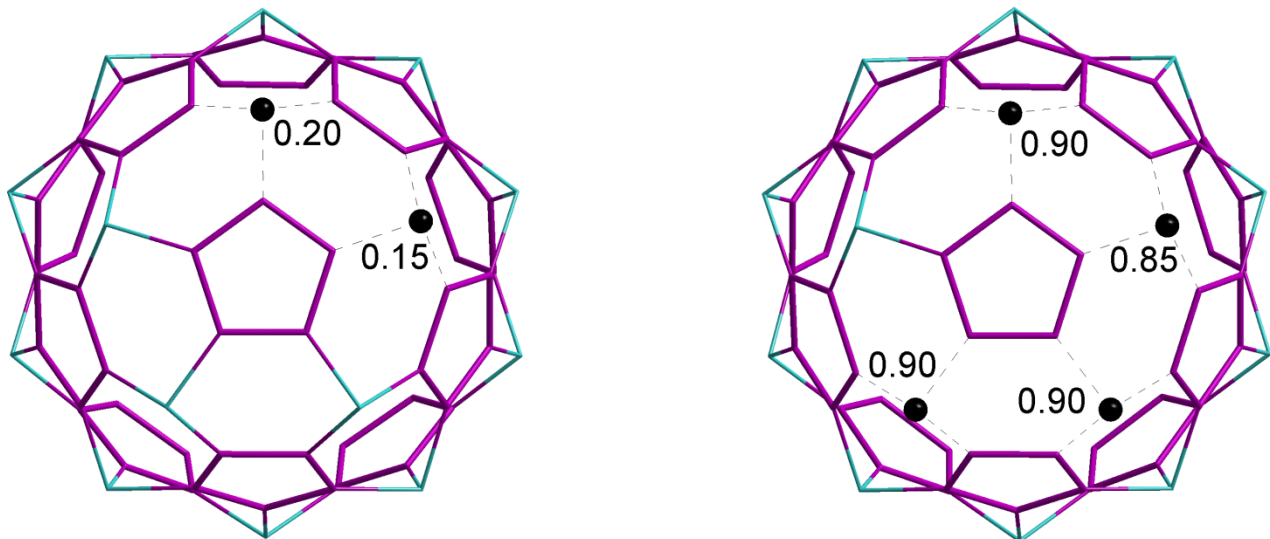


Fig. S24. Schematic view of the experimentally found partly vacant positions of Cu (black balls) in the inorganic scaffolds of supramolecules **1@2a** (left) and **1@2b** (right) with corresponding site occupation factors.

Possible n-vacant supramolecules (**1@2a**: $n \leq 2$; **1@2b**: $n \leq 4$) and their isomers were derived from the type of the disorder of CuX fragments in the inorganic scaffold (Table S5). Specific distribution of the partly vacant positions found in the crystal structure considerably restricts the number of the permutations of the n vacancies over 15 Cu sites and therefore limits the list of theoretically possible isomers of the supramolecules coexisting in the solid state. For example, only one isomer of two possible ones can exist for 2-vacant supramolecules in the case of **1@2a**, as the two vacant positions are located next to each other (cf. No. 3 and 4 in Table S5).

Non-integer composition of **1@2a** and **1@2b** implies not only different composition of the supramolecules, but also the fact that these similar supramolecules with different CuX content can co-crystallize due to their similar shape. Thus, two-, three- or n-component solid solutions of complete and/or incomplete bowl-like supramolecules arise that can have following composition and isomerism listed in the Table S6.

Thus, mutual arrangement of vacancies restricts not only the number of possible isomers, but also some compositions of solid solutions.

Table S5. Individual supramolecules in 1@2a and 1@2b: a reconstruction

No.	Composition of supramolecules	n^*	Molecular structure of possible supramolecules		Coordination of $(Cp^*FeP_5)_5$ fragments at the		
			bottom view	side view	top	middle	bottom
1	$(Cp^*FeP_5)_{11}(CuX)_{15}$ X = Cl, Br complete bowl	0			$5 \times 1,2,3-$	$5 \times 1,2,3,4,5-$	$1 \times 1,2,3,4,5-$
2	$(Cp^*FeP_5)_{11}(CuX)_{14}$ X = Cl, Br	1			$5 \times 1,2,3-$	$3 \times 1,2,3,4,5-$	$2 \times 1,2,3,4-$
3	X = Cl, Br	2			$5 \times 1,2,3-$	$2 \times 1,2,3,4,5-$	$2 \times 1,2,3,4-$
	$(Cp^*FeP_5)_{11}(CuX)_{13}$					$1 \times 1,2,3-$	
4	X = Br	2			$5 \times 1,2,3-$	$1 \times 1,2,3,4,5-$	$4 \times 1,2,3,4-$
	$(Cp^*FeP_5)_{11}(CuX)_{12}$					$1 \times 1,2,4-$	
5		3			$5 \times 1,2,3-$	$4 \times 1,2,3,4-$	$1 \times 1,2,3-$
	$(Cp^*FeP_5)_{11}(CuX)_{11}$					$1 \times 1,3-$	
6	X = Br	3			$5 \times 1,2,3-$	$1 \times 1,2,3,4,5-$	$2 \times 1,2,3,4-$
	$(Cp^*FeP_5)_{11}(CuX)_{10}$					$2 \times 1,2,3-$	$1 \times 1,2-$
7	$(Cp^*FeP_5)_{11}(CuX)_{11}$ X = Br	4			$5 \times 1,2,3-$	$2 \times 1,2,3,4-$	$3 \times 1,2,3-$
	$(Cp^*FeP_5)_{11}(CuX)_{9}$					$1 \times 1-$	

* n is the number of vacancies, i.e. the missing CuX fragment(s) at the 'bottom' of the nano-bowl scaffold. They are shown as black balls.

Possible solid solutions in 1@2a

Higher CuCl-vacant structure **1@2a** generally allows wider range of compositions, which are in the same time highly restricted by existence of only two vacant CuCl positions (Table S2). Here, two and three-component solid solutions can only arise. Among the two-component ones, only 14:13 CuX content of supramolecules is possible, since a 15:13 one would require a ratio of 0.175:0.825 ($15 \times 0.175 + 13 \times 0.825 = 13.35$), which is inconsistent with one of the vacancies of 0.80 (at the position of Cu14), as it is smaller than the required value of 0.825 (Table S6). Therefore, a 2-vacant supramolecule cannot exist in this structure together with only complete ones. More vacant supramolecules are also not possible as there are only two vacant CuCl positions per supramolecule. On the other hand, complete supramolecules (CuCl content 15) can coexist with 1 or 2-vacant ones forming three-component solid solutions. Here, the content of complete supramolecules is limited to 0.15 according to the minimal Cu occupancy in vacant positions, whereas the content of 2-vacant ones is limited to a range of 0.65–0.8. The lowest allowed value 0.65 arises from the composition requirements, whereas the highest value from the minimal Cu occupancy in the vacant positions.

Table S6. Individual supramolecules 1@2a or 1@2b and some of their solid solutions

Inconsistent compositions for solid solutions of supramolecules and impossible isomers are highlighted in red. Major supramolecules are shown in bold.

No.	1	2	3	4	5	6	7
CuX composition	(CuX)₁₅ complete bowl	(CuX)₁₄	(CuX)₁₃		(CuX)₁₂		(CuX)₁₁
n	0	1	2: two isomers		3: two isomers		4
Nano-bowl							
Exists for X	Cl, Br	Cl, Br	Cl, Br	Br	Br	Br	Br
Unknown in eq. 1 and 2	<i>z</i>	<i>y</i>	<i>x</i>		<i>v</i>		<i>u</i>
Composition of solid solutions, %							
1@2a	0.175	x	0.825				
	0.15	0.05	0.80				
	0.125	0.1	0.775				
	0.10	0.15	0.75				
	x	0.35	0.65				
1@2b	0.85	0.05	x	x	x	x	0.1
	0.85	x	x	x	0.15	x	x
	0.85	x	0.05		0.05		0.05
	0.775	x	0.225		x	x	x
	0.75	0.05	0.2		x	x	x
	0.75	0.15	x	x	0.1		x
	0.55	0.45	x	x	x	x	x

In general, the whole range of compositions allowed for solid solutions in **2a** obeys following simultaneous conditions:

$$\left\{ \begin{array}{l} 0.65 \leq x \leq 0.8 \\ 0.05 \leq y \leq 0.35 \\ 0 \leq z \leq 0.15 \\ 13x + 14y + 15z = 13.35 \\ x + y + z = 1 \end{array} \right. , \quad (\text{eq.2})$$

where x , y , z are relative contents of 2-vacant ($13\times\text{CuCl}$), 1-vacant ($14\times\text{CuCl}$) and complete supramolecules ($15\times\text{CuCl}$), respectively.

For example, a ratio of supramolecules $13:14:15 = 0.80:0.05:0.15$ gives correct CuCl content ($13\times 0.80 + 14\times 0.05 + 15\times 0.15 = 13.35$), as well as a ratio of supramolecules $13:14:15 = 0.75:0.15:0.1$ ($13\times 0.75 + 14\times 0.15 + 15\times 0.1 = 13.35$). More possible variants are listed in Table S6.

Possible solid solutions in **1@2b**

In **2b**, the presence of four vacant positions in principle makes possible up to 4-vacant supramolecules of the maximal 0.10 content. The simplest allowed combination is two-component solid solution of the 4-vacant and complete supramolecules. However, realization of 4-vacant supramolecules would require all occupancies for all vacant positions equal, which is not the case. Therefore, the two-component 15:11 solid solution is prohibited. Two-component solid solutions $15:13 = 0.775:0.225$ and $15:14 = 0.55:0.45$ ($15\times 0.775 + 13\times 0.225$ and $15\times 0.55 + 14\times 0.45 = 14.55$) are not in contradiction with the presence of four partly vacant positions with established occupancies (Table S3). However, two-component solid solution of a 15:12 supramolecules in a ratio 0.85:0.15 is allowed from point of view of composition ($15\times 0.85 + 12\times 0.15 = 14.55$), but contradicts the experimental data, because there is no way to fit different orientations or different isomers of 3-vacant supramolecules on 4 vacant positions with experimentally obtained occupation factors.

Three-component solid solutions are restricted to 0.1 part of 4-vacant supramolecules and 0.05 part of 1-vacant supramolecules according to the vacancies distribution. Therefore, resulting 15:14:11 solid solution of a 0.85:0.05:0.1 ratio can exist giving required total CuBr content of 14.55 ($15\times 0.85 + 14\times 0.05 + 11\times 0.1$). Some of other allowed three-component solid solutions are listed in Table S6.

Generally, if u , v , x , y , and z are contents of $(15-n)$ vacant supramolecules with $n = 4$ ($11\times\text{CuBr}$), 3 ($12\times\text{CuBr}$), 2 ($13\times\text{CuBr}$), 1 ($14\times\text{CuBr}$) and 0 ($15\times\text{CuBr}$), respectively, the whole range of compositions allowed for their solid solutions can be described by following simultaneous equations:

$$\left\{ \begin{array}{l} 11u + 12v + 13x + 14y + 15z = 14.55 \\ u + v + x + y + z = 1 \\ 0 \leq u \leq 0.1125 \\ 0 \leq v \leq 0.15 \\ 0 \leq x \leq 0.225 \\ 0 \leq y \leq 0.45 \\ 0.55 \leq z \leq 0.85 \end{array} \right. \quad (\text{eq. 2})$$

Therefore, different interpretations, although a finite number of them, are possible for the disordered average structures of supramolecules **3**.

5 Inorganic scaffolds: a comparison

The novel supramolecules in the shape of nano-bowls are structurally related to two heretofore known supramolecules (Fig. S25). All of them are constructed according to the isolated-pentagon rule^[6] and therefore have fullerene-like topology^[9].

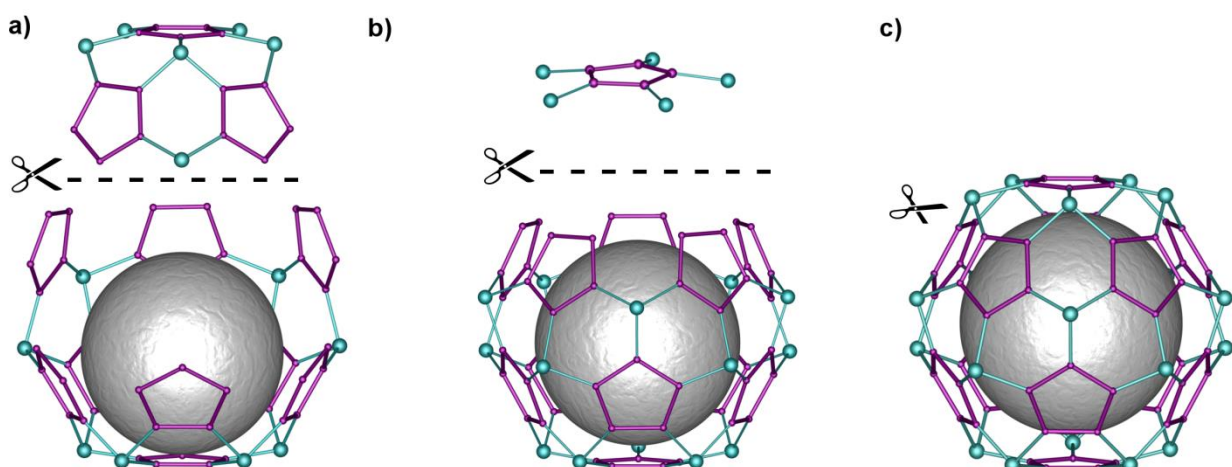


Fig. S25. The structural similarity of the inorganic scaffolds of (a, bottom) an open-shell nano-capsule^[7] and (b, bottom) nano-bowl **2** with respect to the (c) closed-shell 80-vertex supramolecule^[8]. The (a, top) $\{\text{Cu}_6(\text{cyclo-P}_5)_3\}$ and (b, top) $\{\text{Cu}_5(\text{cyclo-P}_5)\}$ fragments are to be eliminated from the 80-vertex scaffold (c) to obtain nano-capsule (a) and nano-bowl (b).

-
- [1] O. J. Scherer, W. Wiedemann, G. Wolmershaeuser, *J. Organomet. Chem.* **1989**, *361*, C11-C14.
 - [2] M. Detzel, G. Friedrich, O. J. Scherer, G. Wolmershäuser, *Angew. Chem. Int. Ed.* **1995**, *34*, 1321.
 - [3] *CrysAlis PRO* 1.171.38.46 (Rigaku OD, 2015)
 - [4] G. M. Sheldrick, *Acta Cryst. sect. C.*, **2015**, C71, 3.
 - [5] A. Schindler, C. Heindl, G. Balázs, C. Groeger, A. V. Virovets, E. V. Peresypkina, M. Scheer, *Chem. Eur. J.* **2012**, *18*, 829
 - [6] H. Terrones, M. Terrones, *New J. Phys.* **2003**, *5*, 1
 - [7] S. Welsch, C. Groeger, M. Sierka, M. Scheer, *Angew. Chem. Int. Ed.* **2011**, *50*, 1435.
 - [8] M. Scheer, A. Schindler, C. Gröger, A. V. Virovets, E. V. Peresypkina, *Angew. Chem. Int. Ed.* **2009**, *48*, 5046-5049.
 - [9] F. H. Hennrich, R. H. Michel, A. Fischer, S. Richard-Schneider, S. Gilb, M. M. Kappes, D. Fuchs, M. Bürk, K. Kobayashi, S. Nagase, *Angew. Chem. Int. Ed.* **1996**, *35*, 1732 – 1734.